UNIVERSIDAD DE CHILE
FACULTAD DE CIENCIAS FÍSICAS Y MATEMÁTICAS
DEPARTAMENTO DE INGENIERÍA ELÉCTRICA

IMPLEMENTATION OF A 300 GHZ TRANSMITTER AND A 2-CHANNEL COHERENT RECEIVER SYSTEM FOR NEAR-FIELD HOLOGRAPHY MEASUREMENTS ON THE FYST TELESCOPE

TESIS PARA OPTAR AL GRADO DE MAGÍSTER EN CIENCIAS DE LA INGENIERÍA, MENCIÓN ELÉCTRICA

PABLO JOSÉ ASTUDILLO ALVARADO

PROFESOR GUÍA:
NICOLÁS ANDRÉS REYES GUZMÁN

PROFESOR CO-GUÍA:
PATRICIO MENA MENA

MIEMBROS DE LA COMISIÓN:
ROLANDO DUNNER PLANELLA
RICARDO FINGER CAMUS

Este trabajo ha sido parcialmente financiado por:
ANID a través del proyecto QUIMAL 180004 y
Centro Basal de Astronomía y Tecnologías Afines (CATA)
a través del proyecto basal FB210003

SANTIAGO DE CHILE
2023

RESUMEN DE LA TESIS PARA OPTAR
AL GRADO DE MAGÍSTER EN CIENCIAS
DE LA INGENIERÍA, MENCIÓN ELÉCTRICA
POR: PABLO JOSÉ ASTUDILLO ALVARADO
FECHA: 2023
PROF. GUÍA: NICOLÁS ANDRÉS REYES GUZMÁN

IMPLEMENTACIÓN DE UN SISTEMA TRANSMISOR Y UN RECEPTOR DUAL COHERENTE PARA MEDICIONES HOLOGRAFICAS DE CAMPO CERCANO EN EL TELESCOPIO FYST

Asegurar una alta eficiencia para el sistema de reflectores de un radiotelescopio es crucial para su funcionamiento. Por este motivo las pérdidas debidas a desviaciones del reflector respecto de su forma ideal deben ser cuantificadas. Para el telescopio Fred Young Submillimeter Telescope (FYST) esta medición requiere detectar desviaciones de 6 um en un área con diámetro de 6 metros, empujando las técnicas de metrología conocidas a nuevos niveles de desempeño.

En este trabajo se expone el diseño, implementación y las primeras pruebas de un sistema de transmisión y recepción para señales de 300 GHz. Se comienza con el diseño a nivel de sistema considerando las características del telescopio. Además, se presenta el diseño e implementación de un sistema para caracterización de antenas a 300 GHz. En tercer lugar, el diseño y construcción de un transmisor de 300 GHz resistente a condiciones atmosféricas. En cuarto lugar, el diseño de electrónica auxiliar. Se finaliza con las primeras pruebas de integración del sistema completo, es decir Front-End junto con Back-End y la electrónica auxiliar. La conclusión de esta ultima medición es que el sistema tiene un tiempo de Allan de 300 segundos, que es adecuado en para su utilización en mediciones de radio holografía.

RESUMEN DE LA TESIS PARA OPTAR
AL GRADO DE MAGÍSTER EN CIENCIAS
DE LA INGENIERÍA, MENCIÓN ELÉCTRICA
POR: PABLO JOSÉ ASTUDILLO ALVARADO
FECHA: 2023
PROF. GUÍA: NICOLÁS ANDRÉS REYES GUZMÁN

IMPLEMENTATION OF A 300 GHZ TRANSMITTER AND A 2-CHANNEL COHERENT RECEIVER SYSTEM FOR NEAR-FIELD HOLOGRAPHY MEASUREMENTS ON THE FYST TELESCOPE

Ensuring a high efficiency in the reflector system of a radio telescope is crucial for its performance. For this reason, losses due to deviations of the reflectors from their ideal geometries must be quantified. In the case of the Fred Young Submillimeter Telescope (FYST) the measurement needs an accuracy of 6um over an area with a diameter of 6 meters, pushing the known metrology techniques to new levels of performance.

This work presents the design, implementation and first tests for a transmission and reception system for signals at 300 GHz. It starts with the system-level design, which includes the telescope characteristics. Then, this thesis presents the design and implementation of a system for characterization of antennas at 300 GHz. Thirdly, the design and construction of a 300 GHz weather resistant transmitter is shown. In fourth place, the design of auxiliary electronics is exposed. Finally, the first integration tests of the entire system is shown, i.e. the Front End with the Back-End and the auxiliary electronics. The conclusion of the former is that the system has an Allan time of 300 seconds, which is adequate for its usage in radio holography measurements.

A mis padres, Guillermo y Susana.
A mi hermana Loreto
... y la Nikita.

Acknowledgements

In first place I want to thank professors Nicolás Reyes and Patricio Mena for the opportunity of working in this project. Also, I want to thank the team at University of Cologne for their support and patience.

I want to give my deep thanks to the people of the Millimeter Wave Laboratory that I have met along the years. They are all exceptional people, and was a pleasure to have shared this part of my life with them. There I found a new and exciting path for my career as an engineer, which allows me to be closely involved in the advancement of science and knowledge. Now, for me, the only direction is forward to discover more and experience life.

Finally, I want to thank my family that has always been there with their love and support.

TABLE OF CONTENT

List of Tables

List of Figures

Chapter 1

Introduction

1.1. Motivation

Since the discovery of radio signals of extra-terrestrial origin by Jansky in the 1930's, the field of radio astronomy has pursued the goal of measuring these weak signals with ever increasing detail. However, as with any measuring device, the instrument itself can degrade the real signal. For the purpose of this thesis the relevant factors for this degradation come from either inefficiencies in coupling the sky signal, or by an addition of an internal error signal due to random processes in the receiver, commonly called noise. Thus, a radio telescope can be more or less sensitive. Losses in sensitivity can be reduced either by averaging the signal over time, or reducing the instrument noise and inefficiencies. Therefore, having more sensitive telescopes would allow for increased mapping speed, and accelerating the advance of science. Thus, antenna and microwave engineering focus on more efficient designs.

The reflector antenna is the main choice for designing radio telescopes, due to its ability to collect signals from a large area and add them coherently in a single point. Several factors can reduce its performance when coupling a signal. One of them, which is the main interest of this thesis, is the physical deviation of the reflectors from their designed shape. If only random errors are taken into account, and not gravitational deflections, for example, the loss in efficiency can be computed using the expression

$$\eta_s = e^{-\left(\frac{4\pi\epsilon}{\lambda}\right)^2} \tag{1.1}$$

Deduced by Ruze in [1], (1.1) relates the antenna surface tolerance efficiency (η_s) with the RMS value of random surface errors (ϵ) and the wavelength (λ). From this expression it is deduced that when $\epsilon = \frac{\lambda}{16}$, the antenna efficiency is reduced by 50%.

Such result imposes a reduction on the performance of radio telescopes, making the surface characterization a critical part in telescope operation. In the case of millimeter wavelengths, measurements using mechanical equipment become impractical for modern antennas. Indeed, at such frequencies, the surface error to be measured can be in the micrometer range over

the large area of the reflector. For this reason several methods that rely on optics, or radio waves, have been developed to characterize surface errors.

Since every telescope has its own particular set of requirements, every reflector metrology system has different implementations. This is specially true in the case of the Fred Young Submillimeter Telescope (FYST), which is particularly novel since it does not use a traditional reflector configuration and has the most stringent surface accuracy requirement over its large reflector area among other radio telescopes. A collaboration between University of Cologne and University of Chile has been formed to develop the reflector metrology system. The latter has been tasked with the hardware integration and characterization, which is the topic of this thesis.

1.2. Hypotheses

Although radio holography is an established technique for measuring a reflector surface tolerance, it has never been used to achieve the levels of accuracy that the FYST project requires. Moreover, the adjustment of two or more surfaces using holography measurements is a completely new field of research. In this work we develop a solution to extend the current limits of the holography technique, with the aim of solving the aforementioned limitations. Our working hypotheses are:

- Accuracy of holography measurements can be improved by increasing the frequency of measurement from 100 GHz to 300 GHz.
- The instrumentation can be based on commercial off-the-shelve (COTS) components. Therefore taking advantage of the latest developments in microwave technologies.
- The two-surface problem that arises from FYST reflector configuration can be solved by parallax, i.e., doing several holographic measurements at different positions of the focal plane.

In the current thesis we focus on the first two hypotheses, i.e., in the extension of the technique to higher frequencies to achieve better resolution. Working at such high frequency requires some additional complexities in terms of phase control and calibration which are tested in the scope of this thesis.

1.3. General Objective

The main goal of this thesis is to design, test and build the holography hardware, with a frequency of operation of 300 GHz. Determine time stability and signal-to-noise ratio is of particular relevance.

1.4. Specific Objectives

To achieve the main goal, several tasks are identified, which are considered the specific objectives. They are:

- Build a 300 GHz source that complies with FYST requirements.
- Design the auxiliary equipment such as power supplies and Local Oscillator.
- Characterize the horn pattern at 295.6 GHz, and check if it complies with the design.
- Test a preliminary version of the system in laboratory, without mapping capabilities. Stability is the main concern in this test.

1.4.1. Scope of the Work

This thesis focuses on the implementation of a technique known as "holography", also referred as "radio holography" or "microwave holography" in the literature. It is a technique that derives the reflector's shape, or rather its deviation from the designed shape, from the phase distribution in the aperture of the antenna. This distribution is reconstructed from the measurement of the antenna's complex radiation pattern.

1.5. Thesis Structure

A review of the state of the art is presented in Chapter 2. First, a history of the techniques developed for surface characterization is covered. Then, an exposition of the most relevant implementations is showed. The discussion continues with the description of the FYST telescope, closing with the requirements for an holographic system for such telescope and the presentation of the proposed solution.

In Chapter 3 the design of the holography hardware will be reviewed, it will cover: optics, RF electronics, auxiliary electronics and a brief mention of the backend and the horn antenna, though they were not part of this work.

In Chapter 4 all experimental characterizations are described, with the setup description, results and analysis. This tests are the horn pattern measurement, the goretex transmission, the oscillator characterization and the end-to-end test.

Finally, the conclusions and future work are discussed in Chapter 5. Because this thesis is part of a larger project, final tests of the hardware will be performed in University of Cologne.

Chapter 2

State of the Art

2.1. Reflector Surface Measurement Techniques

The necessity of measuring ever higher frequencies and/or increasing the spatial resolution of maps have driven an increase in size of the radio telescopes. This increase in size is related to electrical length and usually quantified by the D/λ ratio, where D is the diameter of the primary and λ the wavelength. The increase in the D/λ ratio with more precise surface characterization, has led to the development of several techniques along the years. They will be discussed in this section.

2.1.1. Theodolite and Tape

For the first radio telescopes the main technique of metrology used was the "theodolite and tape". This method, shown in Figure 2.1, used a theodolite in the axis of the paraboloid reflector to measure the angle to a point on its surface and, then, an Invar tape was used to measure the distance from the axis to the point measured. Later, modern laser instruments were capable to give both angle and distance measurements, reporting an accuracy of 100 µm [2]. The main disadvantage of this method is that the reflector has to be pointed to the zenith, thus it does not take into account gravitational deflections [2].

To surpass this limitation photogrammetry and radio holography techniques were implemented for metrology in radio telescopes.

2.1.2. Photogrammetry

Photogrammetry consists of taking several photographs of the dish from different angles, with markers installed previously on the reflector. If enough photos are taken then, using a fitting algorithm, position of the targets and cameras can be calculated. This method has been applied with an accuracy of the order of 30 µm [4]. This technique is still used for telescopes with stricter accuracy requirements, mainly as a first stage calibration prior the use of holography [4].

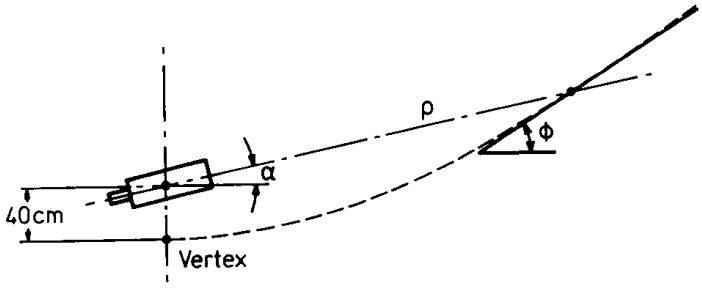

Figure 2.1: Schematic for the "theodolite and tape" technique to survey the shape of the reflector. The reflector, represented by the parabola, is surveyed by the laser which provides angle readings α. Also, the distance from the theodolite to the surface ρ is measured by an Invar tape [3].

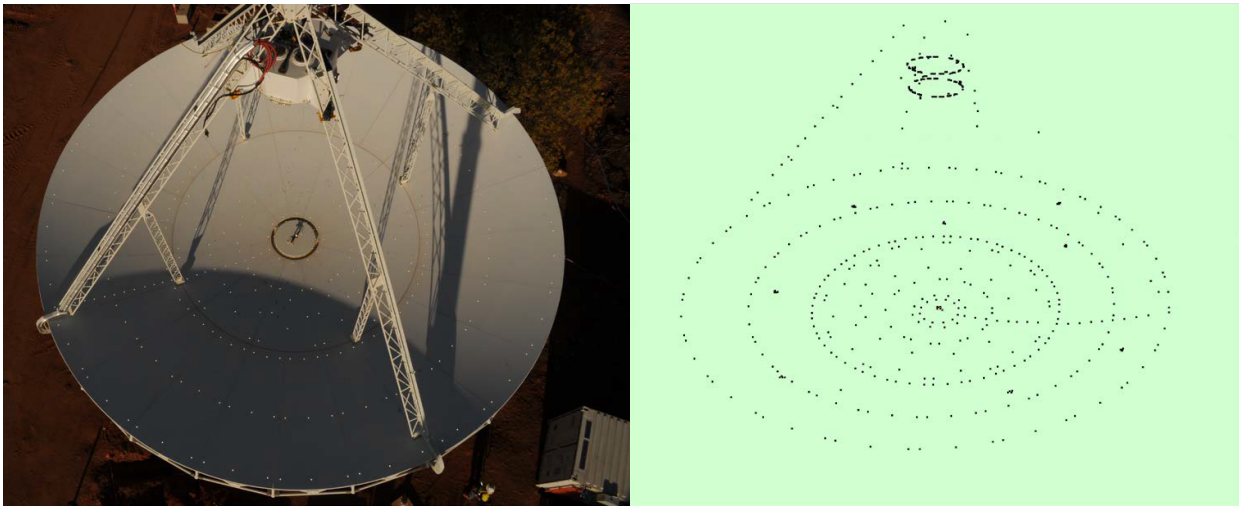

(a) (b)

Figure 2.2: Photogrammetry applied to the ASKAP antenna in Australia. (a) View of the targets placed on the structure. (b) 3D reconstructed model [5].

2.1.3. Radio Holography

This method relies in the properties of aperture antennas, for which it is demonstrated that the radiation pattern of the antenna is the Fourier Transform of the complex field distribution on the aperture [6]. This relation implies that the main goal for the instrumentation is to measure the phase of the radiation pattern. As of today, two methods are found in literature. Here they will be described then shown its uses on radio telescopes.

2.1.3.1. Phase Retrieval Holography

This technique, reported in [7], uses only amplitude measurements of the antenna pattern to calculate the phase distribution in the antenna. The calculation is done using an iterative procedure that assumes an initial aperture distribution and makes corrections using mea-

sured patterns with different foci, until there is convergence within some degree of precision. This method has the advantage of not requiring a direct measurement of a reference signal, which is generally obtained using a secondary antenna. Since most implementations require a heterodyne receiver, this technique can lower costs [7]. Moreover, it does not need hardware for phase measurement, correlators or vector voltmeters. In [8] it is reported that holography via phase retrieval requires twice the observing time, compared to holographic measurements using a reference signal. This makes the measurement more sensitive to changes in temperature and wind conditions. This method has been used in Effelsberg 100-m [8] and IRAM 30-m [9] telescopes.

2.1.3.2. Phase Coherent Holography

This technique relies in the direct measure of the antenna complex pattern, meaning that both amplitude and phase have to be measured. For this reason it is needed to compare two coherent signals, one with information of the antenna optics and the other for reference. The latter is usually a sample of the input signal to the optic system. However, taking a sample of a distant transmitter as reference is impractical, because the antenna field regions (Fresnel or Fraunhoffer) get large for reflectors with high D/λ. Instead, two coherent receivers are used, one receiving the signal going through the telescope optics and the other receiving it directly from the transmitter. Finally, the amplitude and phase difference is computed using a correlator or vector voltmeter as backend. In the first case the phase is contained in the complex cross-correlation of the signals, which is a multiplicative operation. The second case the phase is readily available in the complex phasor ratio of the signals. The ratio measurement has the advantage that it cancels out any variation from the source, however, the reference signal must have a high power and SNR or the amplitude ratio will misbehave [10]. Finally, this is the technique that will be referred as "holography" throughout this thesis.

An important part of the system is the transmitter, where several options have been used, from astronomical sources to ground transmitters, each presenting advantages and disadvantages. Astronomical sources have been used [11], but they do not provide enough power to fully utilize the large dynamic range of the receiver, which is needed to measure the antenna pattern. Because the far-field distance can be as long as several hundred kilometres, at least in the cases considered here, phase coherent holography can be classified by the source position in either far-field or near-field.

In the case of far-field holography, the transmitter has to be at a long distance from the antenna, which poses several implications. One of them is the minimum elevation of the telescope, which makes necessary to use the surrounding geography to position the transmitter. For this reason, satellites are often used as transmitters [8] [9], with its own limitations. One of them is the availability of high orbit satellites, which need to have transmitters at a convenient frequency, a suitable orbit for the elevation range of the telescope and their lifespan are reduced when compared to that of a radio telescope [4]. The second limitation, and relevant for our purposes, is the effect of the atmosphere, which in the range of 300 GHz is quite considerable. Not only the attenuation is a relevant factor but the variability of water content during the day can add errors to the measurement.

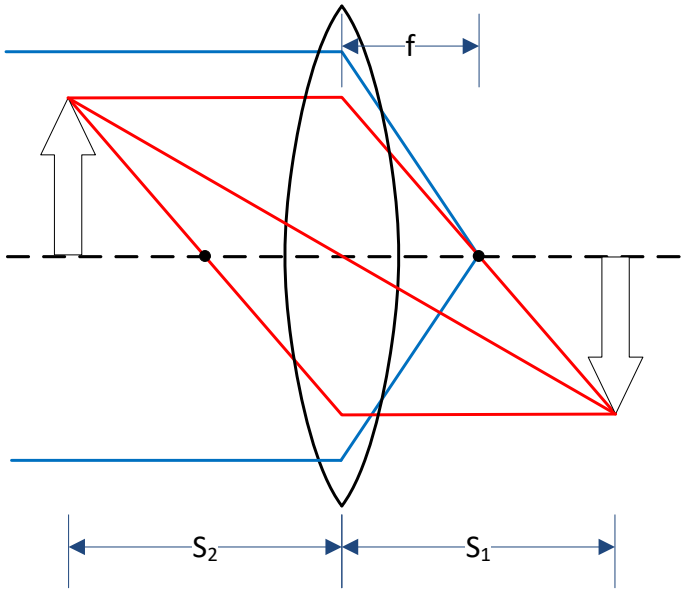

Figure 2.3: Defocusing produced by a source at a finite distance, showing the parameters in equation (2.3). The object is on the left side, and the image on the right. Blue lines are rays from an object at infinity.

A suitable alternative is locating the transmitter in the near-field or Fresnel zone. This implies the use of a different form of transformation between the near-field pattern and the aperture distribution [12]. A shorter distance makes the atmospheric effects less important, but changes in the optical system have to be addressed [4]. More precisely, the defocusing for having a source at finite distance must be considered. This effect consists in the displacement of the image when the object is not at infinite distance, where the image is formed at the focal point, and is similar to the ray optics defocusing. This is shown in 2.3, and described by the thin lens equation,

$$1/S_1 + 1/S_2 = 1/f \tag{2.1}$$

which relates the distance of the object (S_1), the image (S_2), and the focus (f).

According to [4] the major difficulty when using this method are undetected or poorly corrected systematic errors such as an accurate knowledge of the feed horn illuminating the reflector, multipath interference from ground or structure, correct use of the dynamic range of the receivers by avoiding saturation and precise determination of the focal plane.

2.1.3.3. Noise in a phase coherent holography system

To illustrate the constraints of a real phase coherent holography system, a discussion of the limiting factors is presented. In 1982 D'addario [13] developed a noise analysis for two processes: the error in the correlator output due to thermal noise from the receivers and, secondly, the error in the aperture phase distribution due to noise in the measured antenna

pattern.

For the first process, the correlator is modeled as a low-pass filtered multiplicator and the signals are taken as monochromatic of the form

$$\begin{aligned} s_1(t) &= V_1 \cos(2\pi f_0 t) + n_1(t) \\ s_2(t) &= V_2 \cos(2\pi f_0 t + \phi) + n_2(t), \end{aligned} \tag{2.2}$$

where ϕ is the relative phase between the telescope output and the reference and n_i is the receiver thermal noise. By analysing the power spectral density of the multiplication, and assuming that the noise powers $\langle n_i^2 \rangle = kBT$ are equal, then the correlator output signal-to-noise ratio is found to be

$$\mathrm{SNR}_e \approx \sqrt{\frac{\min(P_1, P_2)}{2BN_0}} \cos\phi, \tag{2.3}$$

where P_i is the power of the noiseless signal, N_0 is the receiver noise and B is the bandwidth of the correlator. To be more specific (2.3) is the SNR level for one point in the antenna pattern. This result implies that the noise at the output of the correlator depends on the noise level of the *weaker signal*.

The second error analysis is based on scalar diffraction theory for a circular aperture with uniform illumination, which will be briefly reviewed. If the antenna pattern of the telescope and the reference are noted as $h(u, v)$ and $h_r(u, v)$ respectively, in the uv-space of the infinite sphere, then a measurement of the correlator is

$$M_{ij} = C_0 h(u_i, v_j) h_r^*(u_i, v_j) + \epsilon_{ij}, \tag{2.4}$$

where i, j are the indexes of the pattern in a cartesian map, C_0 is a constant and ϵ_{ij} is the measurement error with $\langle \epsilon \rangle = 0$. If the aperture field is reconstructed from the M_{ij} measurements, it is found that it has non-zero RMS phase error, and depends on the *map signal-to-noise ratio*

$$\mathrm{SNR}_m = \frac{\langle M_0 \rangle}{\sqrt{\langle \epsilon^2 \rangle}}, \tag{2.5}$$

where $\langle M_0 \rangle$ is the average of the on-axis measurement, i.e, the maximum value of the map. It is necessary to point out that correlation measurements are linear for the holographic signal, if the reference is constant. Therefore, when expressing (2.5) in decibels, the logarithm applies to the square of that expression. Finally, if the resolution of the reconstructed aperture field is Δ, then the RMS error in the in the reflector surface position is

$$\Delta z = \frac{1}{16\sqrt{2}} \frac{\lambda D}{\Delta \cdot \mathrm{SNR}_m}. \tag{2.6}$$

These results emphasize the necessity of a high dynamic range for the receivers and backend, besides the required to accurately detect the sidelobes and nulls of the telescope pattern. Expression (2.3) puts a constraint on the reference receiver SNR, which can degrade the measurement. Moreover, (2.6) is very significant in the design because it reveals a trade-off between the resolution in the aperture (D/Δ) and the wavelength to dynamic range of the map ratio (λ/SNR_m), given a certain level of precision.

Finally, since (2.6) assumes a uniform illumination of the reflector, which is non-realistic, it is demonstrated the indirect relation between the noise levels in the signals and the accuracy in the reflector position. A 0 dB taper would introduce error due to reflections with the surroundings, and an uniform phase illumination is very hard to achieve. All these facts imply that a quantification of the accuracy of the system relies heavily on numerical simulations and experimental data. In fact, in [10], using simulations for an antenna with an illumination taper of -13 dB, it was found that the RMS of the surface error was

$$\Delta z = 0.082 \frac{\lambda D}{\Delta \cdot \mathrm{SNR}_m}, \tag{2.7}$$

which is more demanding than (2.6), since $\frac{1}{16\sqrt{2}} \approx 0.0442$. This final expression will be used in this thesis, as it is a more realistic scenario.

2.2. Case Studies

As previously mentioned, the implementation of holography systems is very dependant on the characteristics of the telescope, resources available and target accuracy. Therefore, in this section several study cases are reviewed.

2.2.1. Effelsberg 100m (1999)

In the case of Effelsberg, as described in [8], a phase retrieval holography scheme with a high-orbit satellite beacon as source was implemented. This scheme was chosen because gravitational deformations are a considerable factor, enabling measurements at elevations typical for observations. A new receiver was designed based in an uncooled low noise ambient temperature. A feed with low taper level was used to have sufficient sensitivity in the outer area of the antenna. The specifications of the system are shown in Table 2.1. Some problems of this implementation were reported. The signal transmitted from the satellite showed a frequency drift of 7 kHz, which forced the team to tune the receiver, due to the reduced backend bandwidth. Tracking errors also forced to do calibrations every 30 minutes, having a drift from the predicted coordinates of 4' in azimuth and elevation during one night.

Table 2.1: Holography system parameters, for Effelsberg telescope.

Holography Method	Phase Retrieval
Surface accuracy (detectable)	100 um
Surface accuracy (measured)	500 um rms
Frequency	11.678 GHz
Transmitter	Satellite
SNR	63 dB
Pattern Spacing	35"
Aperture Spacing	1.1 m

Table 2.2: Holography system parameters, for IRAM 30-m telescope.

Holography Method	Far-Field Phase Coherent
Surface accuracy (detectable)	10 um
Surface accuracy (measured)	56 um rms
Frequency	39 GHz
Transmitter	Satellite
SNR	Not reported
Pattern Spacing	35"
Aperture Spacing	13.8 cm

2.2.2. IRAM 30m (2008)

For the case of the IRAM 30m telescope, as described in [9], different techniques were used along the years, but only the 1996-2000 period will be discussed. In those years a phase coherent holography system was implemented, with the parameters shown in Table 2.2. As in section 2.1 a satellite beacon was used as source, both to minimize gravitational deformations and to decrease atmospheric fluctuations by observing at high elevations. The latter consideration is more important when using a 39 GHz signal. A dual receiver configuration was employed, i.e. both reference and holography receiver were mounted in a single rigid, phase-stable structure. Such a configuration enables the use of a single cable for the common Local Oscillator, and only splitting it at the dual-receiver. This assembly was located in the primary focus, replacing the secondary reflector, as shown in Figure 2.4.

A conical horn-lens combination of 30 cm of diameter was used to couple the reference signal with a half power beamwidth of 1.96° by 1.65°, reducing the amplitude taper during a maximum scan angle of 1.6°. To couple the signal from the main reflector a flanged wave feed was used, giving a uniform amplitude and phase illumination. The receivers were implemented with room temperature Schottky mixers with 1200 K of noise temperature. The local oscillator was provided with a phased-locked dielectric oscillator, followed by a tripler. The IF was implemented at stages of 150 MHz, 10.7 MHz and 5 kHz. The latter was chosen to minimize phase errors when carrying the signal over long cables. The bandwidth was set at 3 kHz by crystal filters. An interesting feature of this implementation is a Doppler correction implemented in the digital backend stage.

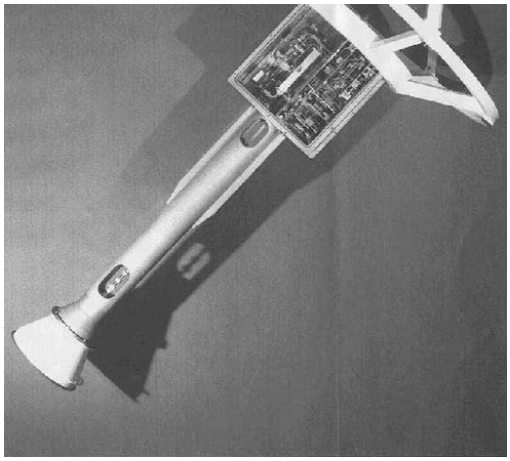

Figure 2.4: Dual receiver used in IRAM holography system, from [9].

Table 2.3: Holography system parameters, for ALMA telescopes telescope.

Holography Method	Near-Field Phase Coherent
Surface accuracy (detectable)	2 um
Surface accuracy (measured)	7.93 um rms (12m), 4.4 um rms (7m)
Frequency	103.8/104.2 GHz
Transmitter	Ground Based
SNR	41 dB (analog), 50 dB (digital)
Pattern Spacing	Not reported
Aperture Spacing	200 mm

2.2.3. ALMA 12m y 7m (2013)

In the case of the ALMA telescopes, as described in [4] and [14], a phase coherent holography system was implemented, with the parameters shown in Table 2.3. The primary objective of the measurement reported in [14] was the study of the reflector thermal deformation over the day. For this reason considerable effort was done to limit other systemic error, like drift in the receiver gains and thermal dilation of the receiver.

The main difference with the system of section 2.2.2 is that a ground-based source was used, giving 8° of elevation from the telescope. This feature limited the capacity to separate gravitational deformations from the effect of misaligned panels in the reflector. As in the case of IRAM-30m a dual receiver located in the primary focus was built. In [14] the use of a dual receiver, made of Carbon Fiber Reinforced Plastic was reported. It was designed to minimize thermal contractions between the signal and reference receivers. The main reason to use this material was the impossibility of using electric heaters to stabilize the structure, because of the mechanical design of the antenna.

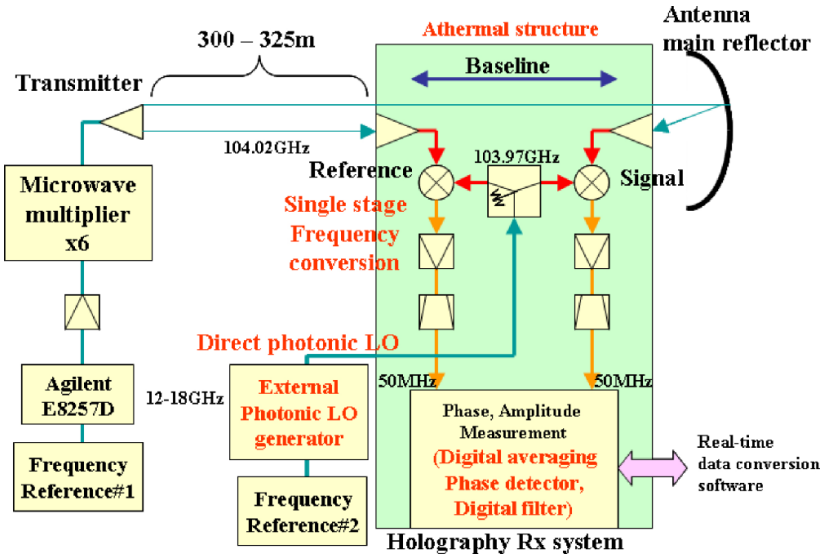

Figure 2.5: Schematic of the holography system used in ALMA, from [14]. The green box represents the dual receiver located at the prime focus. The athermal structure is designed to reduce variations in the distance between the reference and signal feedhorns.

The receivers were implemented in a single-stage frequency conversion, as shown in Figure 2.5, to minimize the distance between the feed antennas. Reflectors were illuminated with a uniform distribution. Millitech biasable balanced mixers and low noise IF amplifiers were used to achieve a noise temperature of 1500 K. Programmable attenuators were used to keep similar power levels between reference and signal receivers. The local oscillator signal was provided via optic fiber, which was downconverted by a photomixer in the receiver assembly. The reasons for this scheme were to minimizing losses in the long distance to the primary focus and ensuring phase stability. The source was a Mach-Zehnder intensity modulator.

2.3. FYST Telescope

The radio interferometers developed in the past 30 years, like ALMA, have added extremely high resolution mapping capabilities to the current astronomical landscape. Moreover, surveying large areas of the sky is still very costly in time and resources. This opens an opportunity, as a complement for those facilities, for an instrument with high mapping speeds and high data throughput [15]. The Fred Young Submillimeter Telescope (FYST) is a single dish instrument specially designed to fulfill this niche because, with its wide field-of-view (FoV), enables the use of large multipixel array receivers.

In this section a brief review of the FYST telescope will be presented, as it is necessary to give the context of the requirements for the holography system. This is specially relevant given the novelty of the reflector configuration.

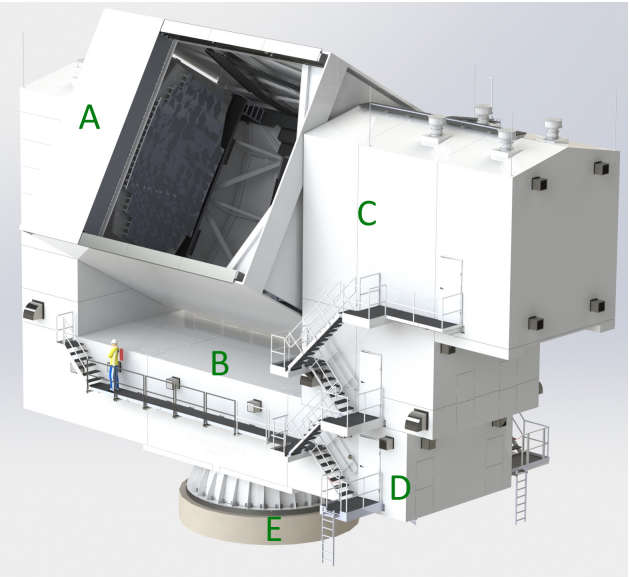

Figure 2.6: FYST mechanical design and its main sections. A: Elevation Housing. B: Yoke structure. C: Primary instrument space. D: Electronics space. E: Support cone.

2.3.1. Main characteristics

FYST is located at 5600 m above the sea level at Cerro Chajnantor, in the high Atacama region of Chile. Within the Parque Astronómico de Atacama, the location was chosen for its extremely dry and cold skies [16], which reduces atmospheric attenuation. In [15] a temperature range of -21 to 9°C is reported as acceptable for normal operation.

The structural design of FYST, shown in Figure 2.6, follows an elevation over azimuth configuration [15]. Both reflectors are located at the "elevation housing", which covers a 180° range in elevation. This housing is supported by the "yoke structure", which covers the 360° range in azimuth and, also, is comprised by several utilities space for electronics and drives. Unlike the telescopes described in previous sections, the detectors are not fixed relative to the reflectors but are static in the "primary instrument space". This is possible because the optical axis for the center beam, after the secondary, coincides with the elevation axis.

The goal of using large multipixel cameras constraints the reflector system in terms of having a large and flat aperture plane with minimum blockage, low cross polarization and low sidelobe levels. To achieve these requirements a crossed-Dragone (CR) system was chosen [17], shown in Figure 2.7, which is an off-axis dual-reflector system. In such a system the surface of the reflectors are described by high-order polynomials (6th and 7th in this case [17]), instead of simple conical shapes used in traditional systems. The coefficients are partly determined by the mechanical parameters of the system but, also, are tuned in such a way that any aberrations introduced by one reflector are cancelled by the other one. The reflectors are designed to provide 7.8° of field of view (FoV), understood as the portion of the sky that maps into the aperture, at a wavelength of 3 mm.

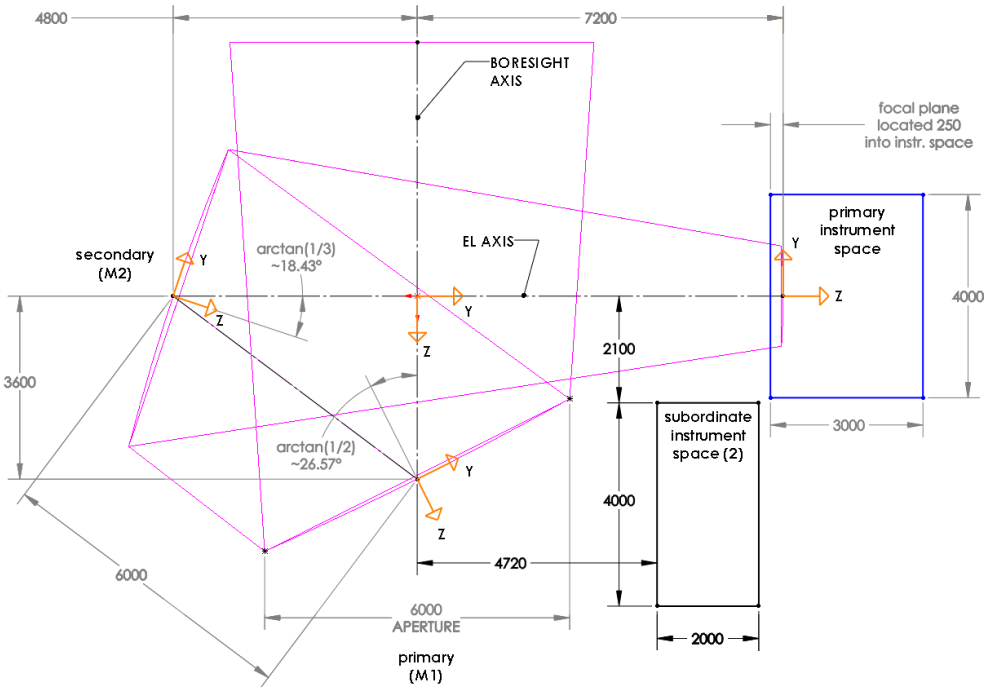

Figure 2.7: Schematic of the reflector system of FYST, taken from [17], all units in millimeters. It is comprised of the primary M1 and secondary M2, which maps the FOV to an aperture of 6m diameter.

Constructing such a shape, with high accuracy at the scale of several meters, makes the use of panels the best option. For FYST this panels are light-weighted aluminum plates, of 675 mm of length, machined from a solid block [15]. They have a backside structure composed of ribs and connection points for 8 adjusters. This adjuster count enables correction of any small distortions from the manufacturing process. The panels are supported by a CFRP-Aluminum structure, which guarantees stability under thermal, wind and gravity loading [15]. The mechanical design is expected to have a surface error of 7.1 µm, below the requirement of 10.7 µm.

2.3.2. Holography requirements

The system accuracy will be set to ensure a maximum error of 10% in the target surface error, which is $\sigma_{ref} = 7$ µm. Considering that these errors are normally-distributed random variables, then the variances add, thus it can be calculated,

$$\sigma_{sys} = \sqrt{\sigma_{tot}^2 - \sigma_{ref}^2} \approx 3 \text{ µm}, \tag{2.8}$$

where $\sigma_{tot} = 7.7$ µm. This error is comprised of both random and systematic errors. If it is assumed a systematic error of 2 µm then, using (2.8) accordingly, the accuracy of the holography system is found to be 2 µm.

To accurately describe the panels of the reflectors, a resolution of 100 mm is taken. Ap-

plying this result into the expression (2.7), for an aperture of 6 m, then it is found that

$$\mathrm{SNR}_m = 0.082\frac{D}{\Delta z \cdot \Delta} \cdot \lambda \approx \lambda \cdot 2.46 \times 10^3 \tag{2.9}$$

or, in dB,

$$\mathrm{SNR}_m = 67.8 + 20\log(\lambda)\ \mathrm{dB}, \tag{2.10}$$

where λ is in millimeters. This result puts a considerable demanding requirement on the SNR of the map, therefore, using the highest frequency possible is desirable. However, commercially available electronics limit the frequency choice to around 300 GHz, or $\lambda \approx 1$ mm. Furthermore, atmospheric attenuation becomes a problem with higher frequencies. Finally, lower frequencies will increase the impact of systematic errors, like a non-uniform phase distribution in the reflector due to the illuminating horn. Therefore, the SNR required for the system is set to 70 dB.

Another important requirement is the speed of the mapping, which is limited by the motors of the telescope. However, short mapping times are needed to minimize changes in the system such as thermal dilation, electronics gain drift and atmospheric attenuation. After having talks with the telescope designers, it was decided a mapping time lower than 20 minutes, which is considered too long to avoid the aforementioned effects. For this reason the sampling of the pattern will consider multiple passes through the telescope's boresight, thus, enabling calibrations to account for any changes in the system. It is projected that these calibrations are taken every 5 seconds.

A final requirement, which is very important but falls out of the scope of this thesis, is that the system must be able to decouple the deviations from both reflectors. This is a novel issue in this kind of measurements because, due to the cross-Dragone configuration, the primary and secondary are similar in size. In previous cases the secondary was much smaller, meaning that it could be excluded from the surface adjustment.

2.3.3. Proposed solution

The method chosen to develop a metrology system for the reflectors of FYST is Near-Field Coherent Holography, as it is the best in terms of achieving the accuracy required. More precisely, result (2.9) imposes the use of a ground based source in the near field, to minimize atmosphere attenuation, and because lower frequencies will demand high dynamic ranges. A summary of the requirements is shown in Table 2.4.

The reference receiver will be positioned in the yoke structure, as shown if Figure 2.8, since it is not possible to replace the secondary by a dual-receiver, like the case of ALMA or IRAM, the chosen position will make difficult to maintain phase baseline. To solve this issue the mapping of the pattern will include several passes through the telescope's optical axis, which will provide a periodic recalibration of the system.

Table 2.4: Holography system requirements, for FYST telescope.

Holography Method	Near-Field Phase Coherent
Surface accuracy (detectable)	2 µm
Surface accuracy (measured)	7 µm
Frequency	around 300 GHz
SNR	70 dB
Transmitter	Ground Based
Pattern Spacing	28"
Aperture Spacing	100 mm
Minimum stability time	5 sec

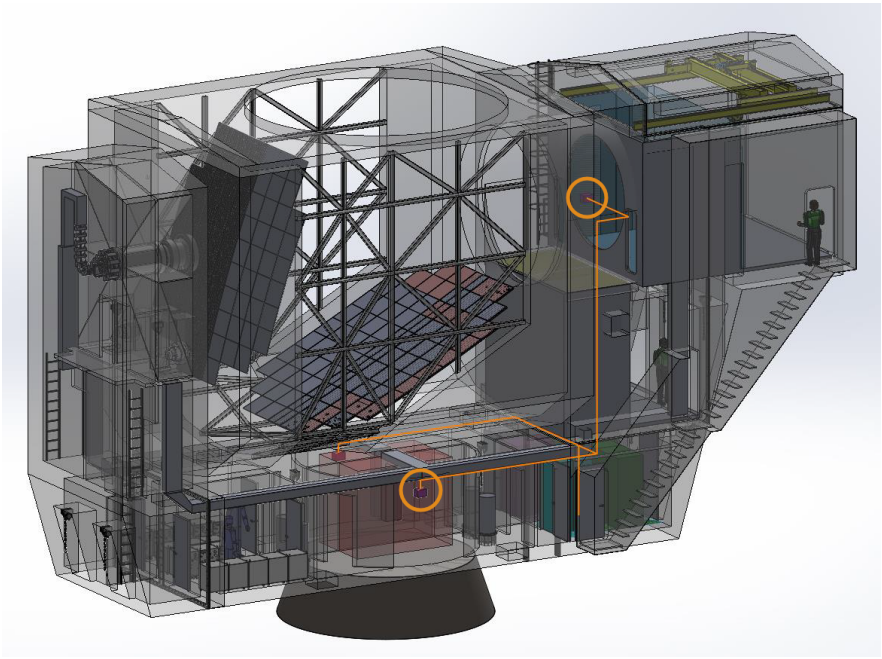

Figure 2.8: Locations of the receivers on the telescope structure, marked by circles. The holography receiver is in the focal plane of the reflector optics, and the reference in the yoke structure.

The position of the receiver is chosen taking advantage of the surroundings of the telescope. Since it sits below the summit of Cerro Chajnantor, it was decided to locate the source by the road that leads to the summit. The main constraint to the distance between source and telescope, which should be close to minimize atmospheric disturbance, is the displacement of the focus mentioned in section 2.1.3.2. The distance from the focal plane and the reflector increases as the source gets closer, to the point that that the latter can collide with the telescope structure. Calculations based on [4] equations determined that 300m is the closest that the source can be to ensure an acceptable clearance with the structure.

To comply with the reflector decoupling requirement, the system will take measurements at different points of the focal plane. This possibility has been demonstrated through simulations [18], and it is planned to test the concept in a laboratory setup at University of Cologne.

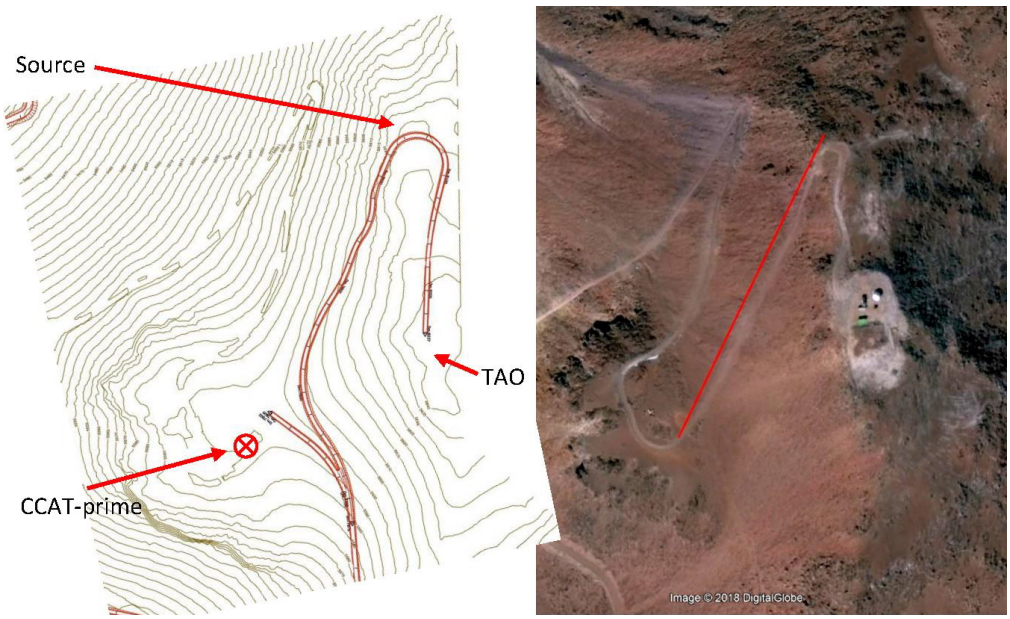

Figure 2.9: Location chosen for source. It is 300m away from FYST projected location, by the road to the summit. It is 3.5m over the telescope, giving an elevation of 3° over its horizon.

As said previously, this thesis covers the detailed design and characterization of the holography hardware. In this way, for the first part, the proposed solution is the development of a COTS 300 GHz RF system, with a source and 2 receivers, using some components developed previously for the project, namely, a 300 GHz horn antenna. The reason for this is that the current commercial landscape offers suitable components as of 2020, which will cut greatly the design stage time. Furthermore, included in the detailed design, is the optic and mechanical design of the source and, also, the design of auxiliary electronics such as power supplies and the specification of the oscillators needed for down conversion and the 300 GHz signal generation.

For the characterization part of the thesis, the solution proposed is the design of several setups using the hardware available in the Millimeter Wave Laboratory (MWL). Of this setups the most important are the measurement of the radiation pattern of the horn, the transmission of the goretex membrane, the characterization of the oscillators and the stability of the whole integrated hardware.

Chapter 3

System Design and Implementation

In this section a review of the design of the hardware is presented, which corresponds to the detail engineering stage. Previous stages were performed by the holography group before the beginning of this thesis, therefore, it is excluded from this chapter. Section 3.1 explains a more general design of the system, before presenting the details of the each part. In section 3.2, the design of the RF electronics of the receivers is shown, however, the mechanical design of the enclosures are not included because they were performed by the team in Cologne. Section 3.3 is about the complete design of the 300 GHz source. In section 3.4, a brief review of the backend designed by S. Jorquera [19] is presented, for the sake of completeness of this thesis. Finally, in section 3.5 the design of the power supplies for the RF modules is discussed.

A brief discussion of the conical diagonal horn is presented, which was designed by R. Molina and based on the results shown in [20].

3.1. General design

As discussed in section 2.3.2 the frequency of operation must be near 300 GHz. At this frequency there are bands identified as being for passive use, including ranges from 275 to 285.4 GHz and 296 to 306 GHz [21]. Therefore, the frequency chosen is 295.6 GHz.

The system is comprised of several units, as seen in Figure 3.1. The RF electronics are divided into 3 modules, namely, the holography source, the holography receiver and the reference receiver. The source will be housed in a small structure, which provides some cover to wind and snow and will have a battery bank and a GPS antenna. Given the position of the receivers, discussed in section 2.3.3, they will be connected to the backend and auxiliary electronics through cables with an estimated length of 15 m for both receivers. The design was focused on generating the final voltages and RF signals within each unit, which minimize the effects of distance between each unit, mainly voltage regulation and phase drift. Finally, all RF modules accept +24 V as input, which simplifies the design of the power supplies units.

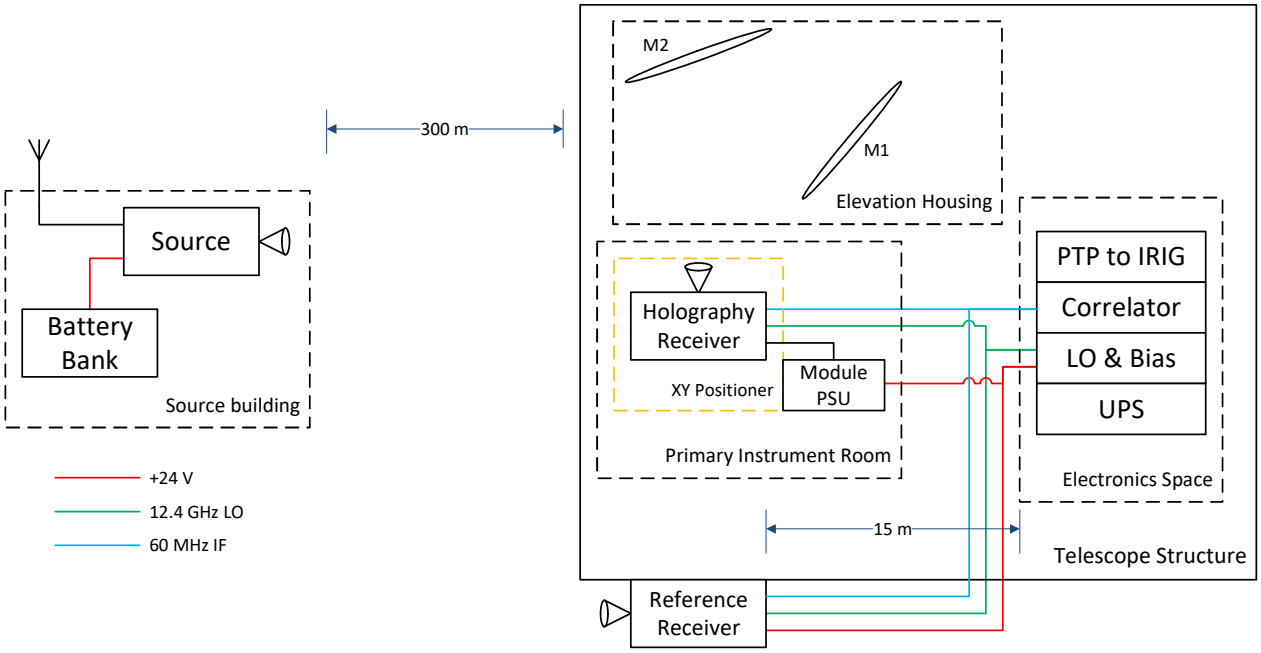

Figure 3.1: General schematic of the holography system. The source is located at 300 m from the telescope, one of the receivers is located at the focal plane while the other one is mounted on the yoke structure. Both receivers are 15m from the electronics space.

The rest of the system consists of the backend and the auxiliary electronics, which are located in the electronics space. This is an enclosed space with a controlled environment, and will hold a standard 19-inch rack for both. The backend is a digital correlator, and has an Ethernet port for communication. The auxiliary electronics are comprised of the LO & Bias equipment, the time and frequency standard equipment and an uninterruptible power supply (UPS). The LO & Bias equipment is a 2U enclosure that holds a +24 V switch mode power supply (SMPS) and a 12.43 GHz dielectric resonant oscillator (DRO), from which the local oscillator for the receivers is derived. The time and frequency standards are provided by a PTP to IRIG converter, which will receive the PTP signals from the telescope timing system, and will provide an IRIG code[1] and a 10 MHz reference for the system. An accuracy better that 1 ms is ensured by the PTP protocol.

The holography system is conceived to be independent from the control system of the telescope, therefore, it is not possible to access data from the telescope pointing system. For this reason, the holography system implements its own timestamp system, which is synchronized by using the timing network of the telescope. Thus, the antenna map will be constructed by crossing the timestamps from the backend data and the pointing system.

[1] Details about the IRIG protocol and its use in the system can be found in [19].

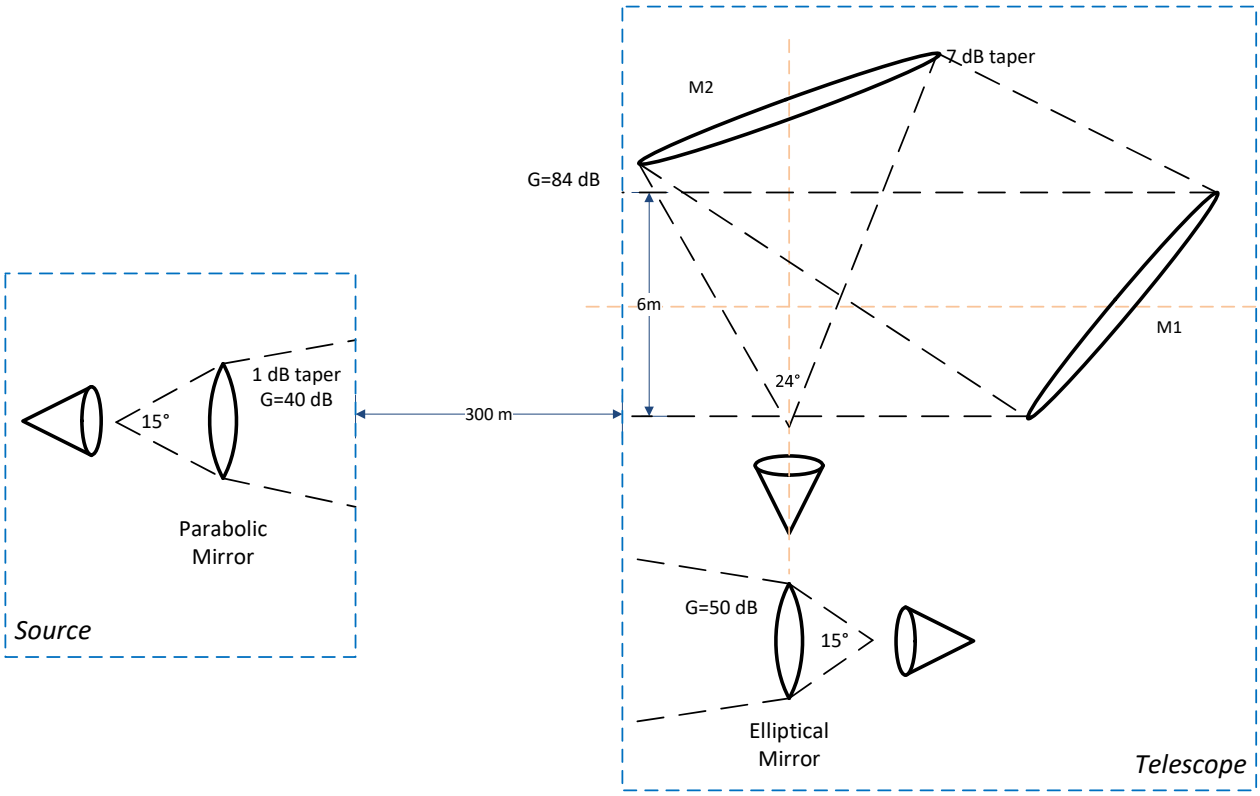

Figure 3.2: Schematics of the optics of the system. Three identical horns are used in each RF module, which was designed to illuminate the telescope reflectors. For the other modules mirrors are used to convert the beams as needed. The source is 3° of elevation over the telescope horizon.

The optical system for the RF modules, as shown in Figure 3.2, uses a Gibson spline horn as the telescope feed antenna, which is shown in Figure 3.3. This type of smooth-walled horn has been shown [22] to be a reasonable alternative to the corrugated horn, which has been the traditional option for radio telescopes. But, in the case of the corrugated horn, because the corrugations are proportional to the designed wavelength, the manufacturing process is very demanding at near-Terahertz frequencies. In [20] it is reported that, at these frequencies[2], it is possible to manufacture a Gibson antenna with -20 dB of cross-polarization, and a Gaussicity above 96%.

The designed horn has the parameters shown in Table 3.1, and it provides a -7 dB taper to the telescope reflectors. This taper is necessary to minimize reflections with the surrounding structures. Simulation results predict a maximum deviation of the phase distribution of 2.86° over the aperture. To avoid designing horns for each unit, thus shortening the designing stage, this horn will be used in the source and reference receiver. Therefore, mirrors have to be designed to adapt the horn beam for the requirements of those units. This mirrors, with parameters shown in the Figure 3.2, were estimated to provide the required dynamic range for the system in a previous design stage.

[2] The antenna was designed for ALMA Band 6 receivers, which cover a frequency range of 211-275 GHz.

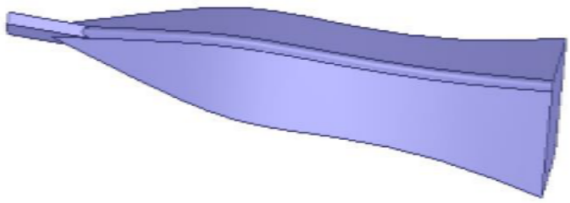

Figure 3.3: 3D model of the spline diagonal horn designed for the holography system. With a length of about 22 mm, its contour is defined by 5 points whose values where determined by optimizing its performance parameters.

Table 3.1: Diagonal spline horn parameters

Full-width at half maximum	15.9°
Beam Waist	1.346 mm
Phase Center Location	1.656 mm
Cross polarization	< -27 dB
Taper at 12°	-7.08 dB
Input Port	WR-3.4

3.2. Radio Frequency Receivers

The design of the receivers, as shown in Figure 3.4, is based on purely COTS components for its electronics. It was decided to use warm electronics without a Low Noise Amplifier (LNA) for the 300 GHz signal, to keep the costs at a reasonable level. The downside of this alternative is the high noise levels introduced by the mixers, therefore, the signal strength of the source must be adequate to ensure an acceptable dynamic range. To mitigate the electronics noise a LNA in the IF path is used, which also bounds noise contributions due to losses in the coaxial cables. The necessity of such amplifier is the main reason to set the IF frequency to 60 MHz, because at lower frequencies shot noise ($1/f$) becomes dominant and increases the noise temperature significantly.

The main RF component is a 220-330 GHz down converter module, which is comprised of a subharmonic mixer with a $\times 12$ active multiplier for the local oscillator (LO). The combination results in a $\times 24$ multiplication thus, if the IF frequecy is 60 MHz, the input LO frequency is 12.32 GHz. A general purpose amplifier is included in the LO path, to compensate for the losses of the final 15 m cable. Finally, the aforementioned LNA is used for the IF signal, to give an adequate power level to the correlator. In Table 3.2 it is shown the noise budget[3] for the receivers, computed using the Friis formula, which shows that the noise temperature is below 5800 K.

[3] The mixer noise temperature is an estimation, due to lack of information of the typical noise temperature of the mixer.

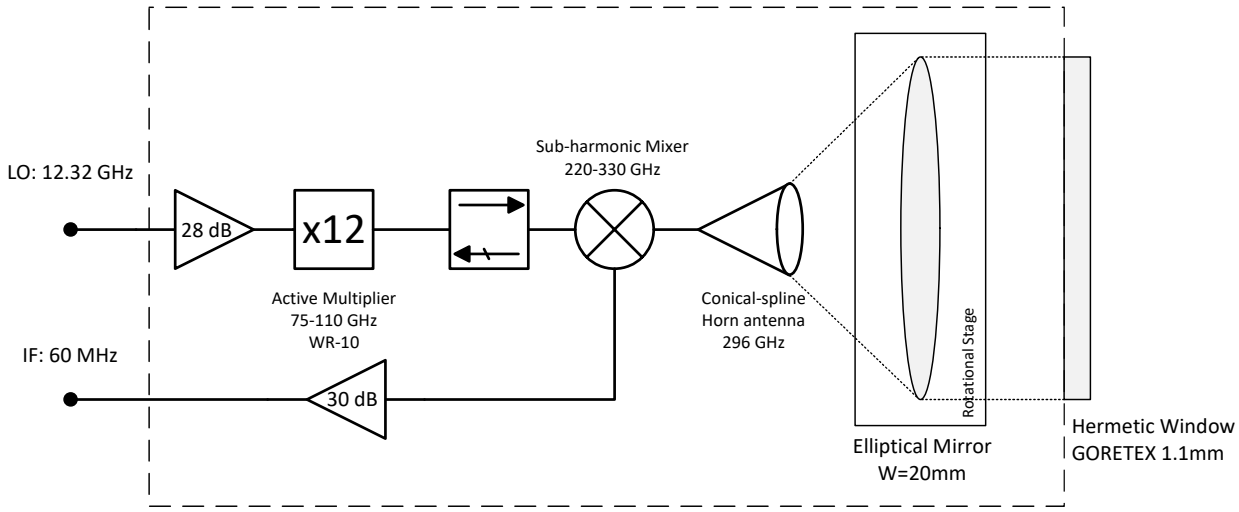

Figure 3.4: Radio frequency receiver schematic for reference signal. It includes mirrors and a rotational stage to maintain boresight to the source. Holography receiver doesn't use any optics but has 60 dB of IF gain.

Table 3.2: Estimated noise budget for the receivers. Negative gain values correspond to losses.

Reference Receiver			*Holography Receiver*		
Component	**Gain dB**	**T_N K**	**Component**	**Gain dB**	**T_N K**
Sub. Mixer	-12	4300	Sub. Mixer	-12	4300
IF Amplifier	30	92.3	IF Amplifier	30	92.3
			IF Amplifier	30	92.3
Total	**18**	**5762.8**	**Total**	**48**	**5762.9**

3.3. Radio Frequency Source

A COTS based source was designed, with rugged design to withstand location weather. As mentioned in section 3.1, the source is expected to face rain, snow and extreme temperatures. It is also expected to run completely independent from the telescope and the rest of the holography system, with only local operation. As the other modules, it accepts a bias voltage of +24V, which will be provided by a battery bank.

The main RF component, shown in Figure 3.5, is a $\times 18$ multiplier chain which, in turn, is composed of an active $\times 6$ and a passive $\times 3$ multipliers. This chain is fed by a 16.43 GHz DRO, which uses a 10 MHz reference provided by a GPS-disciplined oscillator (GPSDO). As it name implies, the GPSDO needs a connection to an antenna to receive the GPS/GNSS signal.

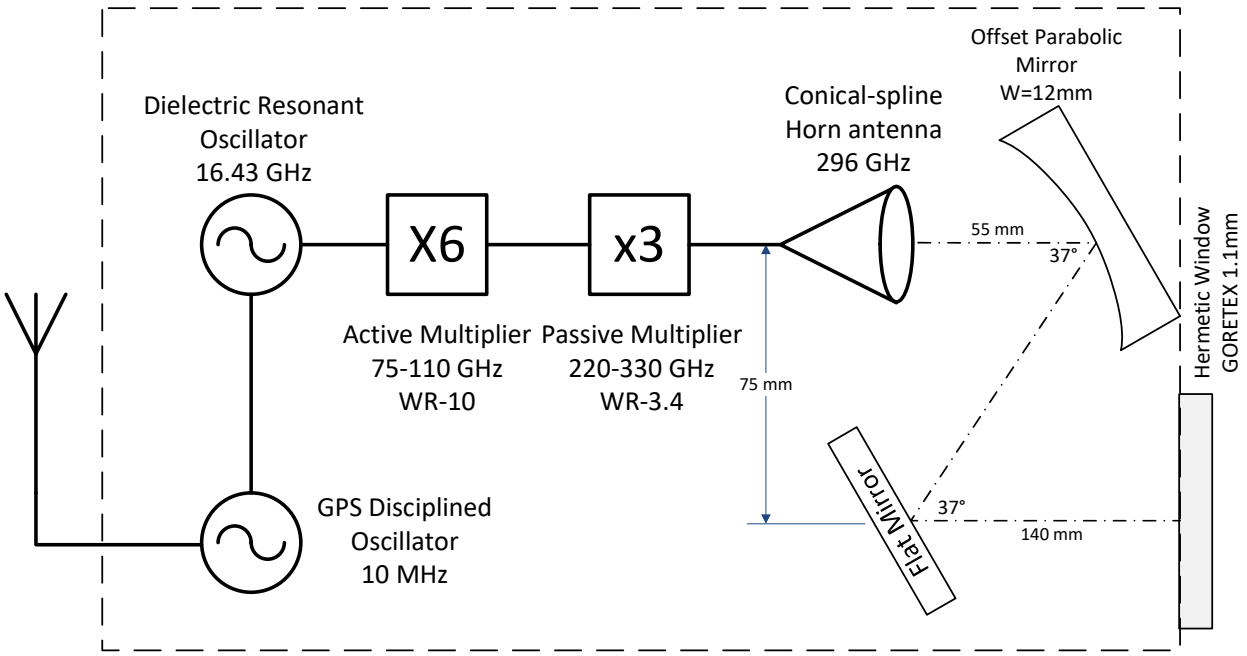

Figure 3.5: Radio frequency source schematic, with a simplified layout of the optics. A gimbal mount is used for fine positioning of the flat mirror.

The optics of the source are designed to provide, at the telescope aperture, an uniform phase distribution and a low-level taper. For these reasons a two mirror system was implemented, where a parabolic mirror collimates the radiation emitted by the horn and, then, a flat mirror is used to direct the beam through the goretex window. This last mirror is mounted on a gimbal positioner, which gives 2 degrees of freedom to fine tune the pointing. This optics are mounted on a slanted plate that tilts the beam down by 2.6° and, also, minimizes the effects of standing waves between horn and telescope. The last is due to the tilt of the goretex window with respect to the optical axis.

An off-axis parabolic mirror was designed to adapt the horn pattern and provide a uniform illumination to the aperture of the telescope. All the equations used can be found in [23]. The edge taper was set to 1.2 dB on the 3 m radius of the aperture and, using this data and the distance to the source, the source beam waist is found to be 12 mm. Therefore, the magnification is around 8.57 and, using the confocal distance of the horn and the fact that the beam waist is located in the focal point of the mirror, the focus of the mirror can be computed as

$$f = \mathcal{M} \cdot z_c = 52 \text{ mm} \tag{3.1}$$

where $\mathcal{M}$ is the magnification and z_c the confocal distance. To obtain the size of the mirror, the beam radius is calculated by

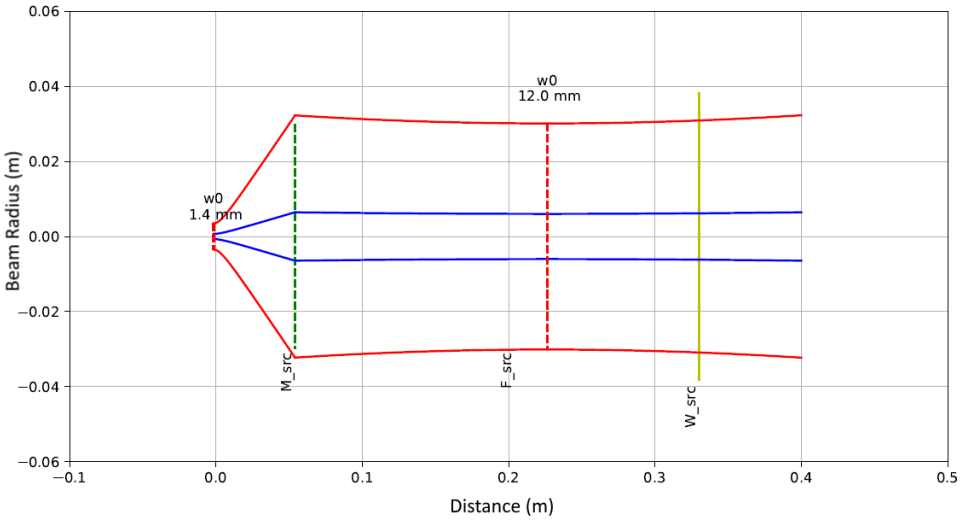

Figure 3.6: Optical train representation of the source optics. Horn beam waist is located at the left, M_{src} marks the position of the parabolic mirror, F_{src} the position of the output beam waist and W_{src} the position of the goretex window. The beam radius (w_0) is shown in blue, and $5w_0$ is shown in red.

$$w(z) = w_0\sqrt{1+\left(\frac{\lambda z}{\pi w_0}\right)^2} \approx 4 \text{ mm} \tag{3.2}$$

where w_0 is the horn beam waist, $z = 52$ mm is the distance to the mirror. To collect most of the transmitted power the mirror will need to cover a diameter of $10w_0$, so 44 mm is taken as diameter for the mirror. The angle of the mirror must be set to satisfy the relationship

$$\frac{r \cdot \sin\theta_i}{f} \ll 1 \tag{3.3}$$

where r is the radius of the mirror, θ_i is the angle between the incident ray direction and the normal direction of the mirror, and f the focus. To comply with this criteria $\theta_i = 18.5°$ is chosen, which means that the output collimated beam has a 37° angle with the input. With this data the focus of the parent paraboloid (f_P) of the mirror is

$$f_P = f \cdot \cos^2\theta_i \approx 49.3 \text{ mm} \tag{3.4}$$

Finally, an offset of 75 mm between the horn and flat mirror axis, and the goretex window is 140 mm in front of the flat mirror. In Figure 3.6 is shown the evolution of the beam in the optical system, from this it is straight forward that the diameter of the goretex window has to be 70 mm to transmit the beam without obstruction. Also, following the same criteria the diameter of the mirror is set to 75 mm.

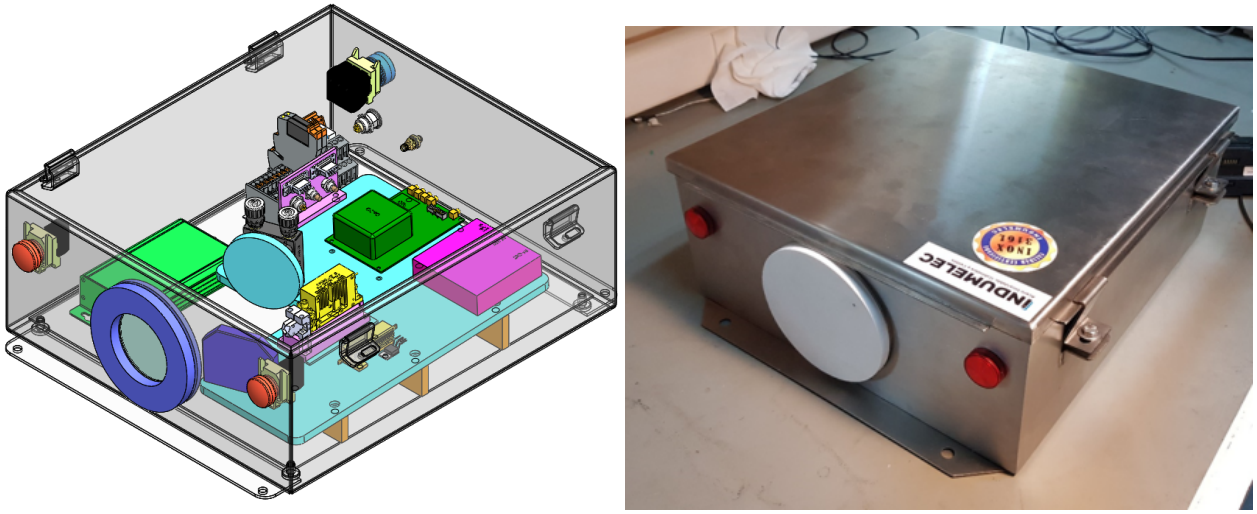

(a) (b)

Figure 3.7: (a) Source 3D mechanical model, isometric view. External enclosure not shown or transparent to reveal internal components. At the front the lights and the window can be seen, the latter shows the goretex membrane (gray green) and the o'ring flange (blue). At the back a push button switch an the connectors for the bias and GPS antenna. (b) Picture of final assembly. The enclosure has four perforations to fix its position on a platform.

The mechanical design of the source, as shown in Figure 3.7.a, uses a stainless steel NEMA 4X standard enclosure as it provides water tightness and resistance to corrosion. With a dimension of 400 × 350 × 150 mm, the enclosure includes a mounting plate on which the source electronics are mounted. Custom perforations were made to fit the external components (i.e. connectors, switches and pilot lights) and a large perforation for a window to transmit the signal. To seal the window a goretex membrane is used, due to its low transmitting losses at millimetric wavelengths. To ensure water tightness, all components that interface with the exterior have sealing o'rings. The final enclosure is shown in 3.7.b and has a net weight of 15 kg.

As mentioned in section 2.3.1, the temperature range for normal operation of the telescope is between -21 and 9°C. For this reason all sensitive electronics are temperature stabilized using an isolated plate, shown in Figure 3.8, with a simple heater. The heater is a simple analog design, with an Operationa Amplifier (OPAMP) receiving as input a reference set by a potentiometer and the reading of a temperature sensor. The OPAMP chosen has a high current stage, thus it can drive the aluminium housed power resistor that acts as heating elemet. This plate is isolated from the rest of the enclosure by using Nylon PA66 spacers between optics and mounting plates.

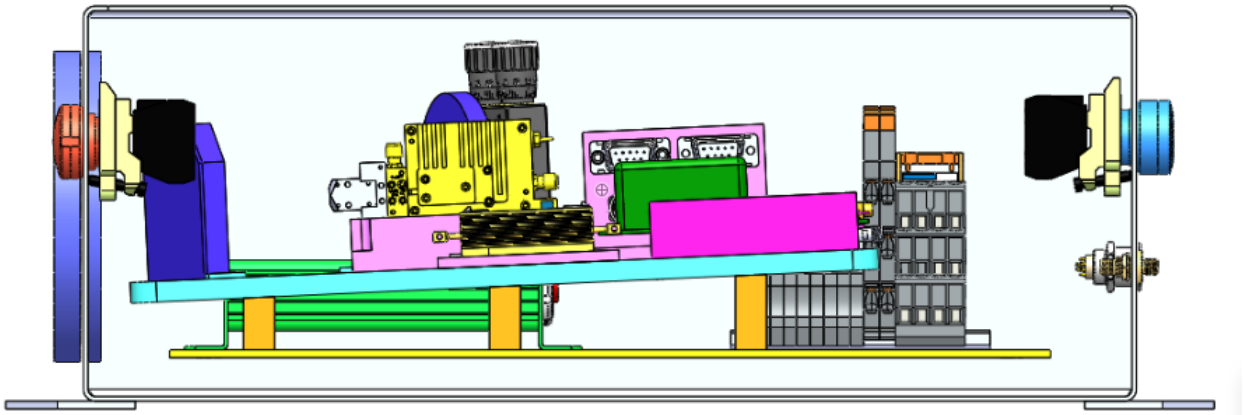

Figure 3.8: Side view of the source. Above the bottom side of the enclosure is the mounting plate, shown in yellow. Nylon spacers, shown in orange, are between the mounting plate and the optics plate, shown in cyan. Behind the optics plate the power supply is shown in green.

Besides the RF electronics and power supply, the source requires other features for its operation. The first one is light signaling of the lock status of both the DRO and GPSDO and, secondly, a manual switch to turn all the RF electronics except the GPSDO to save energy while the latter is locking to the GPS signal. For this features it was chosen to use only industrial DIN components, to simplify the design and manufacture processes. DIN relays and opto-isolators were used to provide electrical isolation between the chassis components (i.e. pilot lights and switch) and the internal electronics.

3.4. Backend

For the holography project a digital correlator was developed by S. Jorquera [19], with parameters shown in Table 3.3, and implemented on the Reconfigurable Open Architecure Computng Hardware 2 (ROACH2). This FPGA-based platform has a high data processing power, and is commonly used for real-time computations of large Fast Fourier Transform (FFT).

To achieve the 70 dB of dynamic range, needed by the holography system, the design relies on the 2.16 GSa/s 8-bit ADC of the platform. Because the expected IF signal frequency is 60 MHz, the ADCs oversamples this by a factor of 16. The use of decimation allows to decrease the bandwidth while increasing the dynamic range of the correlator. This is further increased by the intrinsic gain of a large FFT and time integration (accumulation). Aliasing is prevented by using analog low-pass filter with 70 MHz cut-off frequency. Finally, the accumulators can be configured for integration times between 1 to 20 ms.

Table 3.3: Backend parameters, from [19].

Bandwidth	67.5 MHz
Channel BW	8.24 kHz
FFT Size	16384 sa
Min. Time Resolution	0.485 ms
SNR ($\sigma \leq 1°$)	70 dB

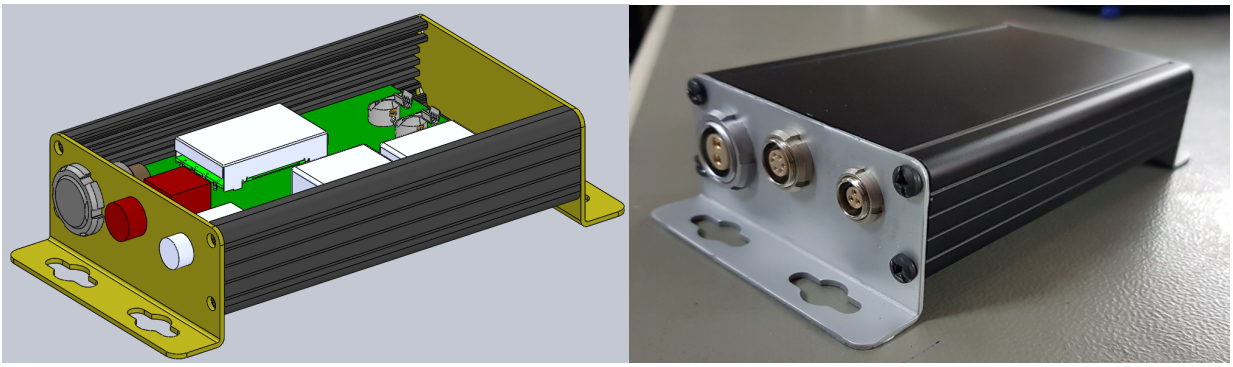

(a) (b)

Figure 3.9: (a) Power supply 3D mechanical model, isometric view. All connectors are located at the front panel, shown in yellow. The input connector (+24V) is shown in gray, the rest are outputs. The top lid has been removed show internal components. (b) Picture of final assembly. The board is inside an extruded aluminum enclosure and fixed by the panel connectors to the front side.

Another feature of the design is its high between-channel isolation, which is implemented by windowing the signal using Poly-phase Filter Banks (PFB). Also, as mentioned in section 3.1, it implements a time stamping system based on IRIG-code protocols. This protocol was chosen as it is a single ended signal that can be fed into the general purpose input of the FPGA, where the signal is decoded by a finite state machine.

3.5. Power Supplies

The use of DC/DC converters was chosen since 24V lines are used to distribute power and, then, produce the final voltages at each unit. This enables to get high efficiencies, specially when the output voltage is considerably lower that 24V. Also, it makes the conversion to negative voltage possible. However, the major drawback is the presence of AC components due to the switching electronics used on this devices, around 5 kHz, which could contaminate the spectrum of the signal with a high harmonic of the switching frequency.

The design considers using this power supplies either within the enclosure of the modules, or in the primary instrument space of the telescope. Therefore, no measures were taken to make them weatherproof. The mechanical design can be seen in Figure 3.9.a, and the

final assembly in Figure 3.9.b. Also, electronics are rated to work within the operating temperature range of the telescope. Another consideration in the design is the election of capacitors, since SMPS need to handle switching currents and capacitors with extremely low Equivalent Series Resistance (ESR) are needed.

Finally, a simple scheme of protections for over-voltage and under-voltage was implemented on each of the boards. There are three reasons for this, the first one being the high cost of the RF electronics. The second one is to match the input range of the converters which, if not done, could result in a partial turn off of the modules if the input voltage gets too low. Finally, the third reason is to give more immunity to transients in the input voltage, which is a feature integrated in the LTC4367IMS8 IC.

3.6. Summary

The detailed design of the metrology system is presented, along the the design of the receiver, source and auxiliary electronics. Both the source and the dual receiver RF electronics are COTS based. The system is designed to operate independently from the astronomical instrumentation and control software of the telescope, only using its time reference network for synchronization. The source was completely designed, but only the RF electronics were specified for the receivers. The auxiliary electronics were designed to run the RF modules on a +24 V supply.

Chapter 4

System characterization

In this chapter the discussion is centred in the different setups built to characterize the holography hardware, with a presentation and analysis of the obtained results. Section 4.1 describes the measurement of the radiation pattern of the horn at 300 GHz, which was the first time measurements at such frequencies were done in the laboratory. Section 4.2 presents the setup to measure the transmission of a goretex membrane, used in the holography source as window. In section 4.3 the characterization of the Dielectric Resonant Oscillators (DRO's) is discussed, whose stability are of particular importance for the system. Finally, section 4.4 describes the final test, called end-to-end test, in which all the components are integrated and its stability is characterized.

4.1. Horn pattern

For this type of experiments, similar to holography measurements, the relative phase between the Antenna Under Test (AUT) response and a reference signal has to be measured. Previous setups at the MWL took the reference from a sample of the source, using a directional coupler at the frequency of transmission. Since such components were not available at 300 GHz, the holography scheme was adapted for this measurement. This can be seen in the schematics in Figure 4.1.

Though the original experiment contemplated the use of the final holography hardware, this soon turned to be unattainable at the moment, due to the contingencies of year 2020. For this reason two Virginia Diodes (VDI) modules were used, namely, a frequency generator extender and a spectrum analyser extender. The first module has a total multiplication factor of $\times 18$. The second one is a spectrum analyser extender, i.e., a down-converter from 300 GHz with an LO multiplication factor of $\times 48$. One of the final down-conversion modules was used to obtain the reference signal. However, because this module has a $\times 24$ multiplication factor it was necessary to use intermodulation products of the second harmonic of the LO, therefore, matching the factor of the other down converter. To achieve a good SNR for the reference signal, both IF low noise amplifiers were used, giving a gain of 60 dB approximately. Finally, the reference receiver used another of the diagonal horn antennas built for the project, giving an additional 20 dB of gain. This provided 15 dB SNR, in spite of higher conversion losses.

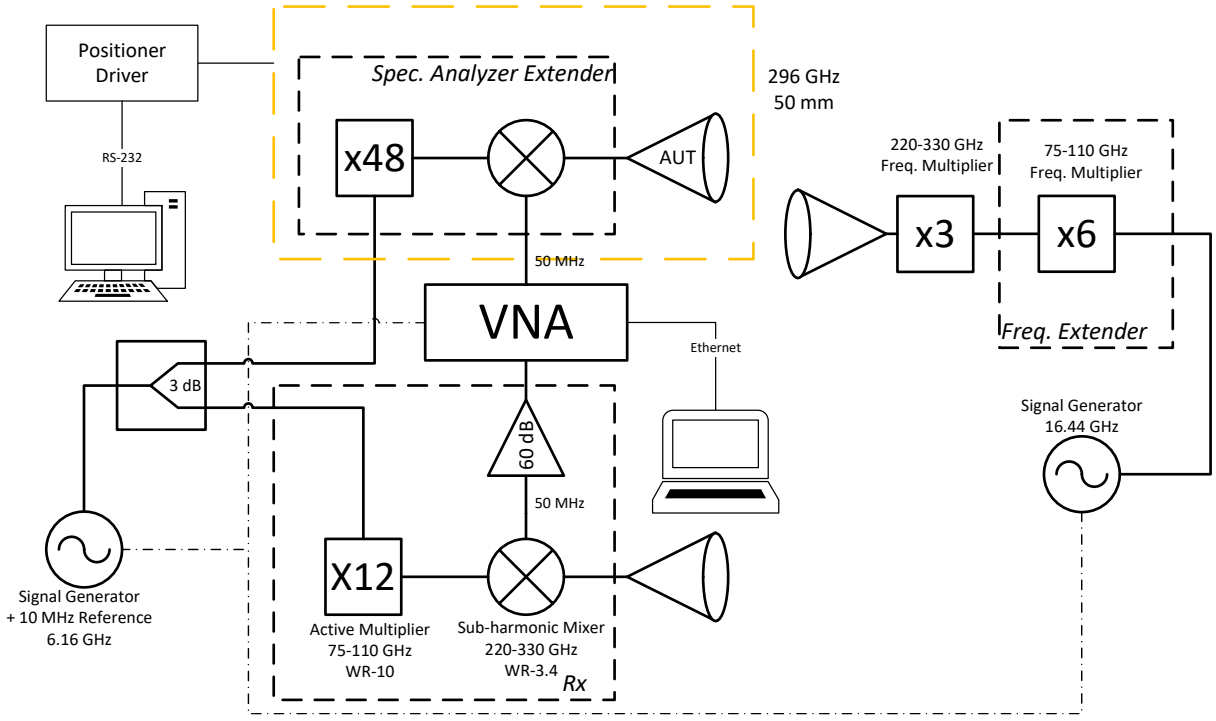

Figure 4.1: Setup schematics for horn antenna measurement. The test signal is generated by a signal generator and a 300 GHz frequency extender and transmitted by an open-ended waveguide probe. This signal is coupled by two antennas to their correspondent receivers. The AUT (up) is mounted on a planar positioner, represented by the yellow box, to map the pattern. The second antenna (down) is a fixed antenna, which gives a stable reference signal. Both IF signals are measured by a VNA, which computes the phasor ratio.

Using gaussian beam propagation theory the size of the plane can be estimated for the beam waist of the horn, as shown in Table 4.1. Given that the side lobes of the diagonal conical horn are rotated 45° from the horizontal plane, the scan plane size can be reduced to a 100 × 100 mm square. Also, the distance to the AUT was chosen to give enough dynamic range (40 dB SNR) while not saturating the receivers, since 300 GHz absolute power instrumentation was unavailable at the moment. This final requirement was checked by measuring several cuts of the beam, each with a different power input at the source, and then comparing to see if the gaussian beams are showing power compression near the boresight.

An on-the-fly mapping scheme was implemented to reduce measuring time, avoiding thermal drift on the electronics and making the measurement more robust. To implement this a simple time sweep was programmed in the VNA but, because it can measure at a much faster rate than the required to satisfy the Nyquist criteria for a reasonable scan speed (lower than 30 mm/s), the approach was to down sample the trace obtained by the VNA. Synchronization at the start of each line of the scan was ensured by using one of the digital outputs of the positioner controller as external trigger of the VNA.

Table 4.1: Parameters of the anechoic chamber measurement. All units in millimetres, unless otherwise specified.

Optics		**Mapping**	
Beam waist (w_0)	1.4	Sampling factor	0.48
Lambda	1.01	Sampling distance	0.485
Confocal Distance	6.07	Number of points	207
Distance DUT	50	Scanning speed (mm/s)	5
Beam Radius at 50mm (w)	11.62	IF Bandwidth (Hz)	40
Plane size ($2 \times 5w$)	116.22	Final plane size	100

Also, care was taken to program the length of the VNA sweep to match the travel time of one line. To do this, the RF settings of the VNA are set (specially the IF Bandwidth) and then the cycle time is measured[4] with a given number of points. Depending on the time measured, the number of points is adjusted and the VNA and positioner are matched. High accelerations can be used in the XY stage due to its mechanical stiffness, therefore, it can be assumed that carriage is moving at a constant velocity and that an equispaced array can represent the spacial distribution of the trace.

The system uses two computers: one communicating with the driver via RS-232, and a second one acting as the user interface of the program. This last one sends high-level commands to both the positioner computer and the VNA to execute a scan. To ensure that no commands were sent to the Postioner Driver while executing a line of the scan, the existing code of the positioner computer was modified so it listens to a return signal from the driver, and sharing this status with the monitoring computer. To avoid having the positioner computer stalled while waiting for the signal from the driver, the serial listening was carried by a second process at the same computer. This enables to send abort commands from the monitoring computer, and also querying other driver parameters if needed.

A picture of the setup can be seen at Figure 4.2, where both receivers and the source are shown. The positioner is a combination of a XY linear stage and a rotational stage, to allow for a roll motion and measure crossed polarized patterns. The position of the reference receiver is relevant in this setup, since it has to provide a good SNR while avoiding blocking or introducing reflections to the other receiver. The source is mounted on a rotary stage to ensure that its boresight is perpendicular to the scanning plane. A semi raster scanning pattern was performed, where the measurement is done only in one direction and returning to start the next row. This avoids an interlacing effect in the pattern due to the flexing of the cables.

Use of the setup showed that the main difficulty of this measurement is the drift in the receivers, which changes the conversion losses in a scale of 30 minutes approximately. Stability measurements were performed to determine that a 20 minute scan was the best mapping time, avoiding both vibration and drift.

[4] The cycle time differs from the sweep time, since the former only accounts for the observation time of the signal. The latter includes switching times for the internal LO, filter convergence, etc.

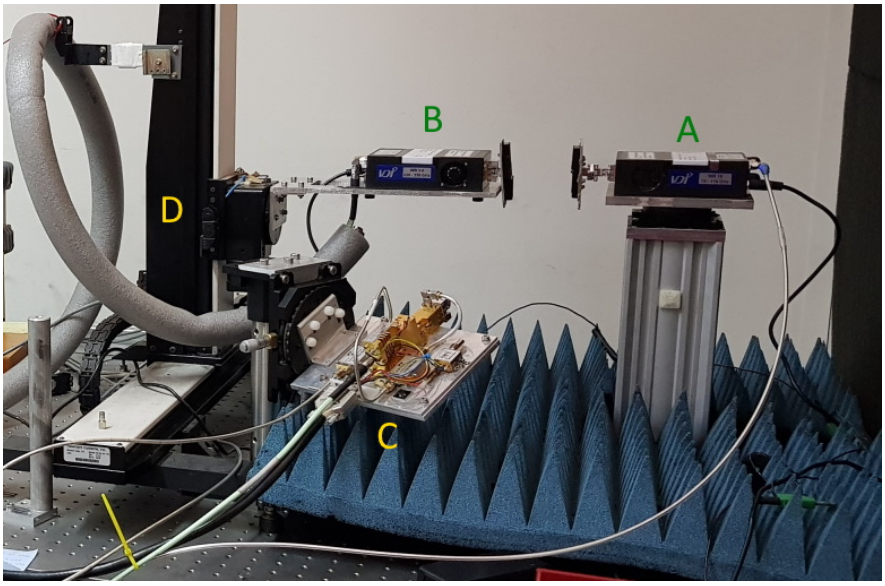

Figure 4.2: Picture of the horn measurement setup. A: 300 GHz source with probe. B: Spectrum analyzer with AUT. C: 300 GHz reference receiver with horn antenna. D: 2-axis linear stage.

Table 4.2: Summary of measured parameters.

	HPBW [deg]	**PCL [mm]**	**24° Taper [dB]**
H-plane	14.6	55.9	-6.9
E-plane	15.3	55.1	-7.3
D-plane	14.4	56.1	-7.5

The results of the copolar measurement are shown in Figures 4.3.a and 4.3.b as bi-dimensional maps and cuts in the relevant orientations respectively. The main issue that can be observed is the presence of a "ringed" structure on the pattern, which is thought to be a small reflection from the structure of the setup. Although bigger reflections were successfully removed with use of electromagnetic absorber, this remnant reflection could not be suppressed due to the lack of sufficient absorbent rated for 300 GHz.

Computing the far field transformation of the previous patterns gives the results shown in Figures 4.4.a and 4.4.b, as maps and cuts respectively. From this data it can be observed that sidelobe levels are below 25 dB, and are mostly present in the diagonal direction. The half power beam width (HPBW) can be computed by gaussian fitting of the main lobe. Phase center location (PCL) was computed using the least-square fitting for the phase described in [24]. The value suggests an average PCL of 5.7 mm behind the aperture, which differs from the 1.656 mm obtained by the simulations in the design stage. This can be explained by the lack of a precise measuring method to set the distance between probe and DUT, which is more critical in this setup because at this wavelengths a precision better than 1 mm is needed. This results are shown in Table 4.2, where it can be concluded that the beam is symmetrical.

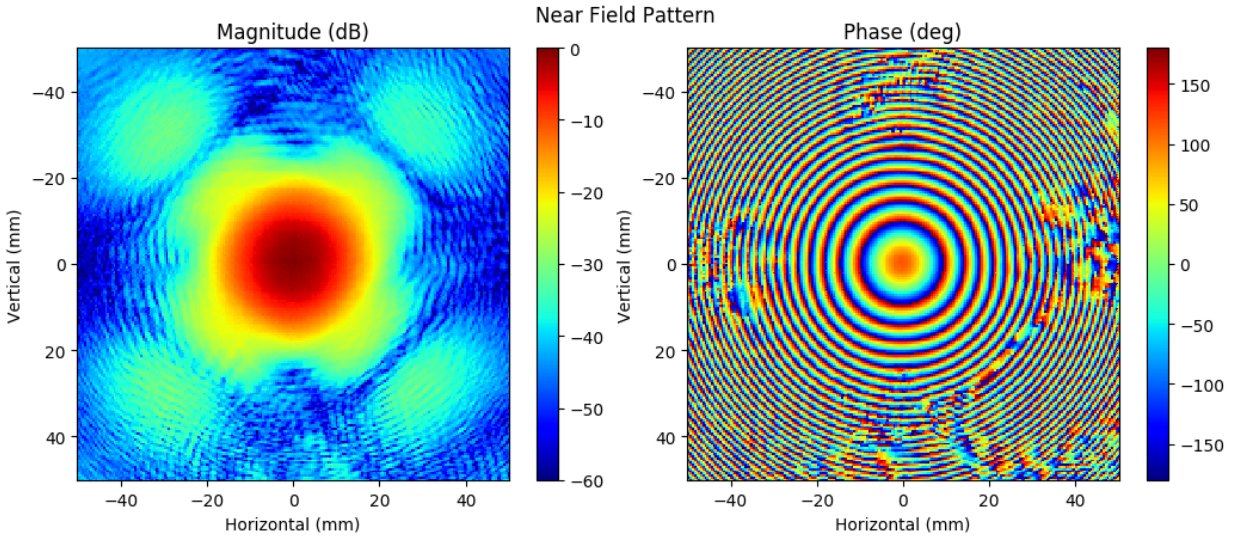

(a)

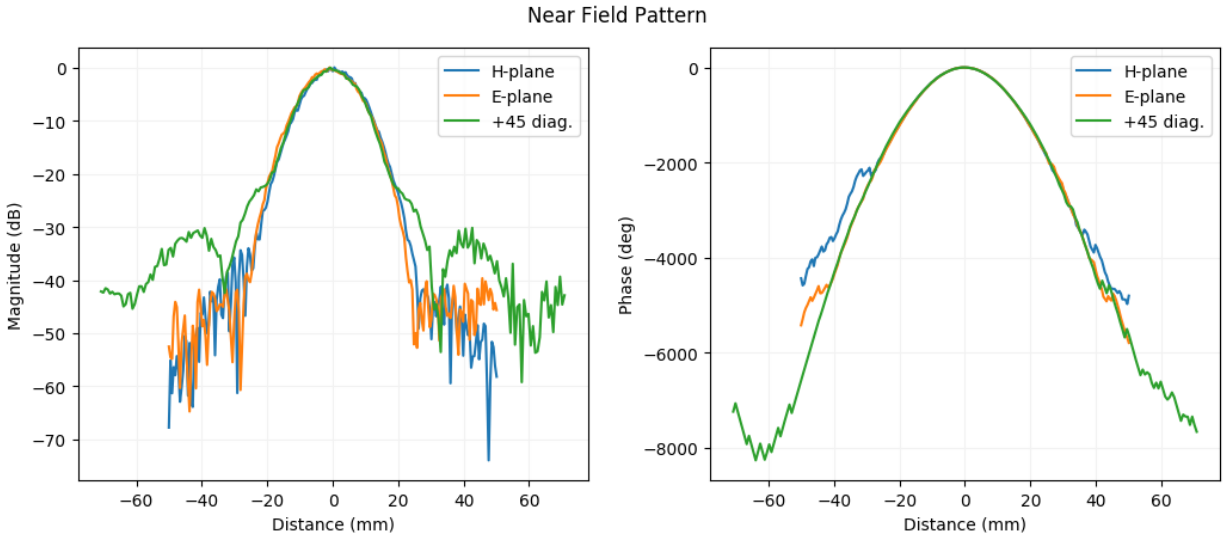

(b)

Figure 4.3: Measured 296 GHz near-field pattern of conical-spline horn. (a) 2D map in amplitude and phase. (b) Cuts in several planes, amplitude and unwrapped phase.

A comparison with the simulations performed by R. Molina can be seen in Figure 4.5, on the most relevant planes. From this it can be concluded that the horn manufactured is compliant with the original design.

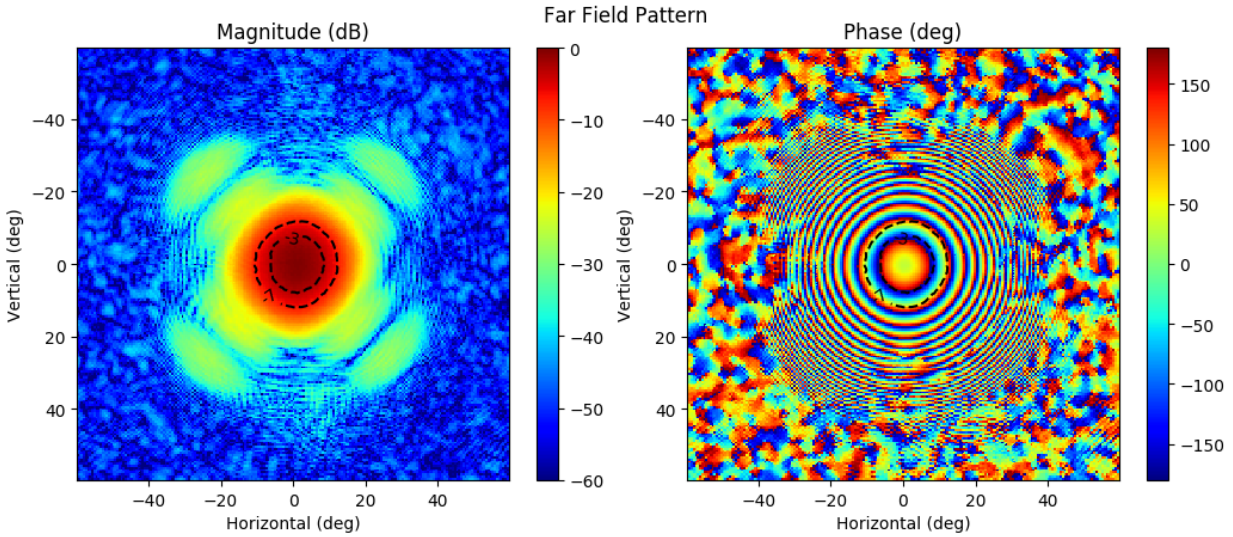

(a)

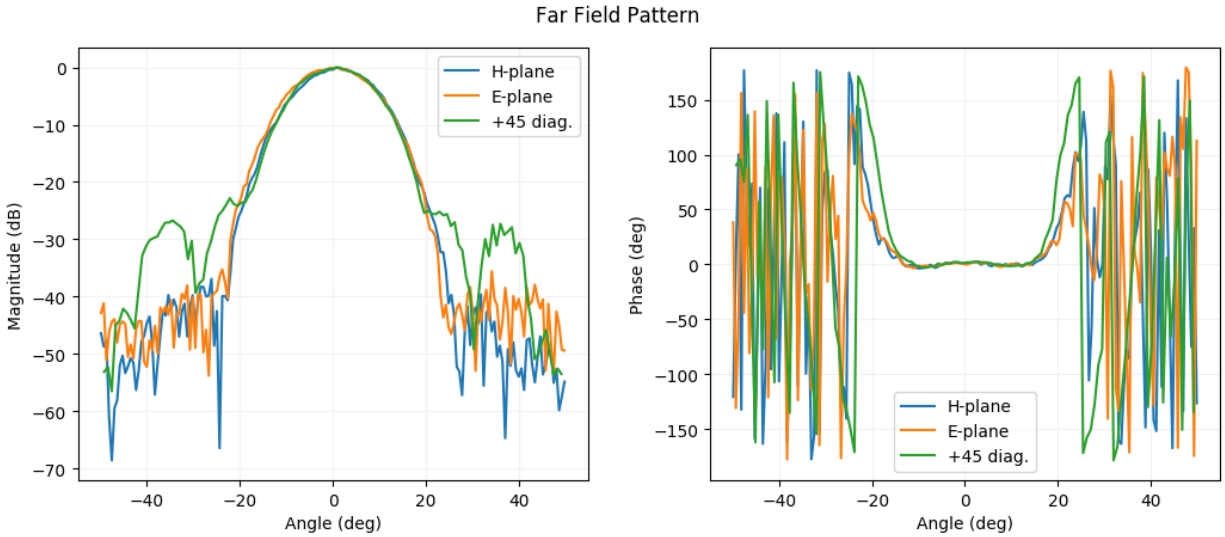

(b)

Figure 4.4: Transformed far-field pattern of conical-spline horn. (a) 2D maps for amplitude and phase, in both is shown the contour levels corresponding to the HPBW and the edge taper. (b) Cuts in several planes, with corrections for phase center location.

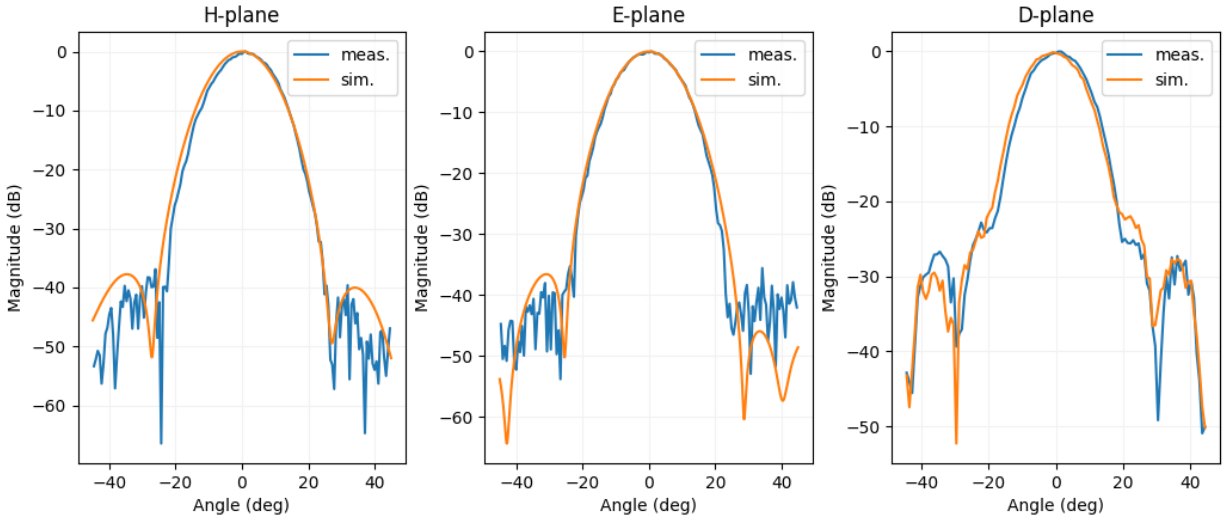

Figure 4.5: Comparison between measured and simulated horn patterns, in multiple planes. D-plane stands for a $\phi = 45°$ cut in spherical coordinates.

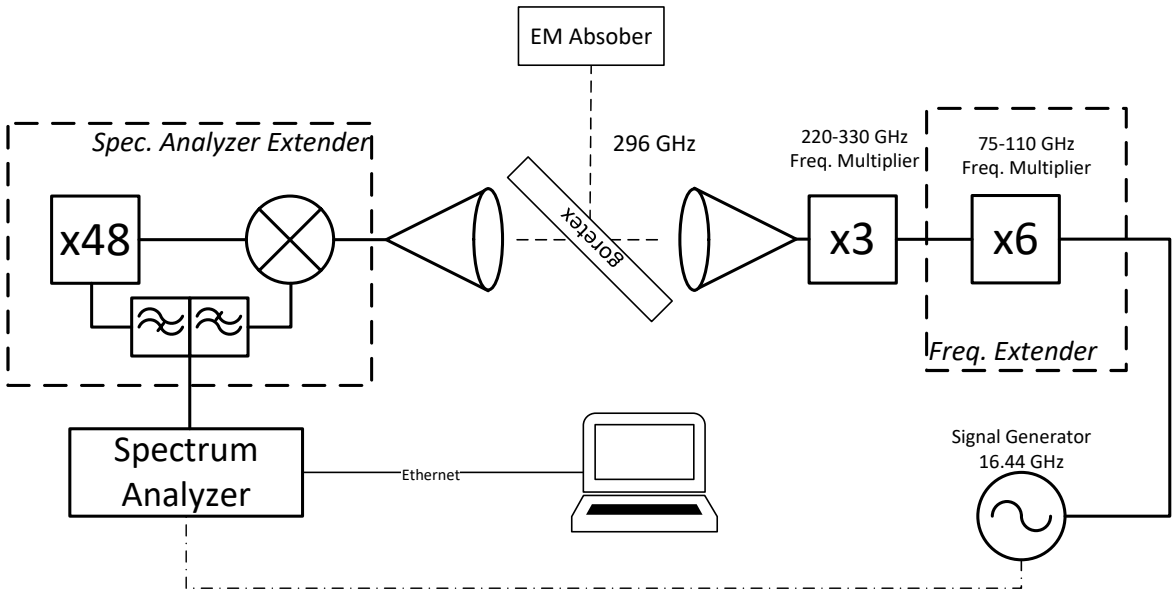

Figure 4.6: Setup schematics for goretex transmission measurement. A 296 GHz test signal is generated using a laboratory signal generator and a frequency extender module. The signal is coupled using two spline-conical horns, the spectrum is measured with a Spectrum Analyzer. A piece of goretex is located between at an angle to avoid reflections. Finally, an electromagnetic absorber is used to avoid reflections with the walls.

4.2. Goretex transmission

An unguided wave was transmitted to measure the transmission of a Goretex membrane with thickness of 1.1 mm, as shown in Figure 4.6, to then quantify the insertion loss. The advantage of this method is that specific hardware is not necessary, like a waveguide filled with the material, on the other hand the down side is the introductions of reflections with the surroundings. As this is a relative measurement a calibration must be done without a the goretex membrane present, which is the baseline for the loaded measurement.

As shown in the schematics, the goretex membrane was placed at an angle of 45° with respect to the line of sight between transmitter and receiver, which avoids reflections between optics and the membrane. Another issue of this setup was the reflections between source and downconverter, due to the mismatch of the non-linear devices, i.e., mixers and frequency multipliers.

The system is comprised of a Spectrum Analyzer to get the power readings, a signal generator to drive the active multiplier chain and emit in the 300 GHz range. The signal is down converted by the same module used in the horn pattern measurements of section 4.1. A monitoring computer sends instructions to both analyzer and generator, using SCPI over Ethernet, to then synchronize a frequency sweep between 290 and 300 GHz.

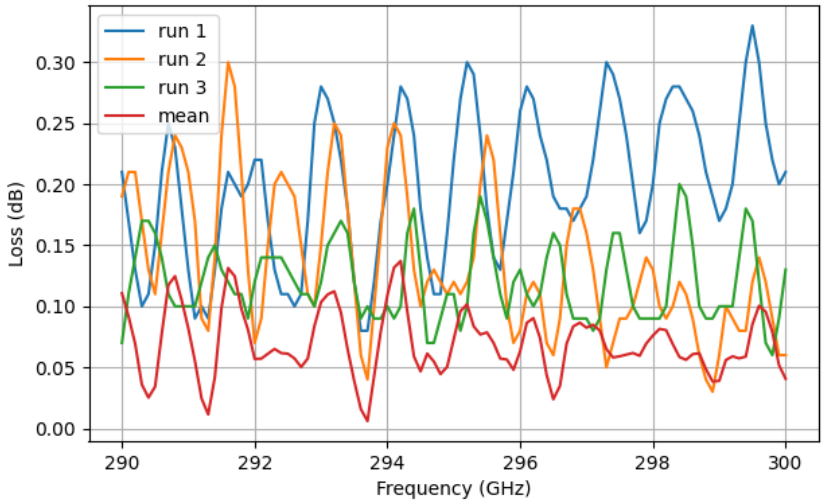

Figure 4.7: Measured loss for several runs. Due to the reflections with the surroundings, the mean (red) is computed and taken as a more accurate measurement of the real loss.

The results of the measurement are shown in Figure 4.7, for several runs. The presence of a standing wave is evident in the graph, which could not be completely eliminated. A possible explanation could be internal reflections in the material, or the lack of enough electromagnetic absorbent rated for 300 GHz. Also, the variability between curves can be explained due to the lack of use of an optical table when assembling the setup. Considering that the wavelength is around 1 mm, any deviation of the position of orientation of the components can modify the electrical length of the optical path. By taking the average of the runs it can be found that the losses of the goretex membrane is 0.07 dB at 295.6 GHz

4.3. Oscillator characterization

A relevant requirement of the system is the phase stability, which can degrade the sensitivity of the system. For this reason the spectral purity of the oscillators is important, both for the source signal generation and the down-conversion process. Both frequency and phase stability were characterized in the laboratory. These tests are straight forward, but nevertheless important for the system.

The spectrum of the oscillators were measured, shown in Figure 4.8.a and Figure 4.8.b. The instrument used for this is an N9030A spectrum analyser from Agilent Technologies (now Keysight Technologies), which has a remarkable high dynamic range and low phase noise. This instrument presented some problems with its auto-calibration mechanism, which makes absolute power measurements invalid, but it is still useful to characterize spurious signals and phase noise as they are relative to the carrier. Also, the spectrum measured has a narrow bandwidth, therefore, the change in gain/loss of the components inside the instruments are negligible. This spectra show that the receiver oscillator has spurious signals 67 dBc and the source oscillator below 48.28 dBc. It is important to mention that the oscillator of the source had the 10 MHz reference from the GPS reference.

To measure the phase noise spectrum, i.e. $\mathcal{L}(f)$, the same spectrum analyser was used, but the detector was set to RMS. This provides a better representation of channels with noise, since the default detector looks at the spectrum of each channel and chooses the maximum value if there is a tone detected, or alternates between maximum and minimum for channels that only have noise. As the RMS detector name implies, it computes the root mean square of the spectrum of each channel, underestimating the value of single tones. To account for this the phase noise spectra is computed using information from spectra using both the default detector and the RMS detector. From Figure 4.8.a and Figure 4.8.b the measurement results can be observed in logarithmic scale and compared with the specification values. It can be noted that the 12 GHz oscillator is close to specifications, except for the 100 Hz point, which can be explained by the width of the channel set in the spectrum analyser. This was 220 Hz, the minimum possible for the instrument, and makes impossible to obtain the 100 Hz point. Finally, it can be observed that the 16 GHz oscillator doesn't comply with the specifications.

Another characterization performed with the oscillators is the frequency stability, which was measured using a frequency counter, with a resolution up to 1 Hz. As the aforementioned measurement, the setup is straightforward, but it is important to mention that the frequency counter must be locked to the oscillator being measured. The results are shown in Figure 4.9.a and Figure 4.9.b, for the receiver and source oscillators respectively. Several curves were measured, but only a window from the steady state is shown for each oscillator because is the most relevant state for the final system. From this results it can be concluded that they have a variation better than ± 0.2 ppb.

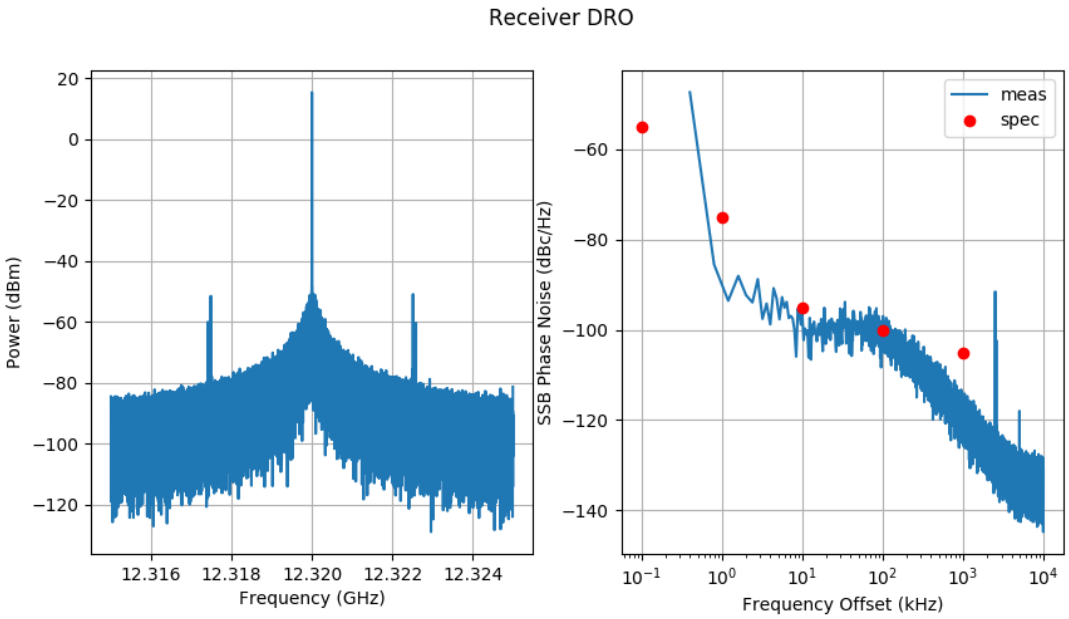

(a)

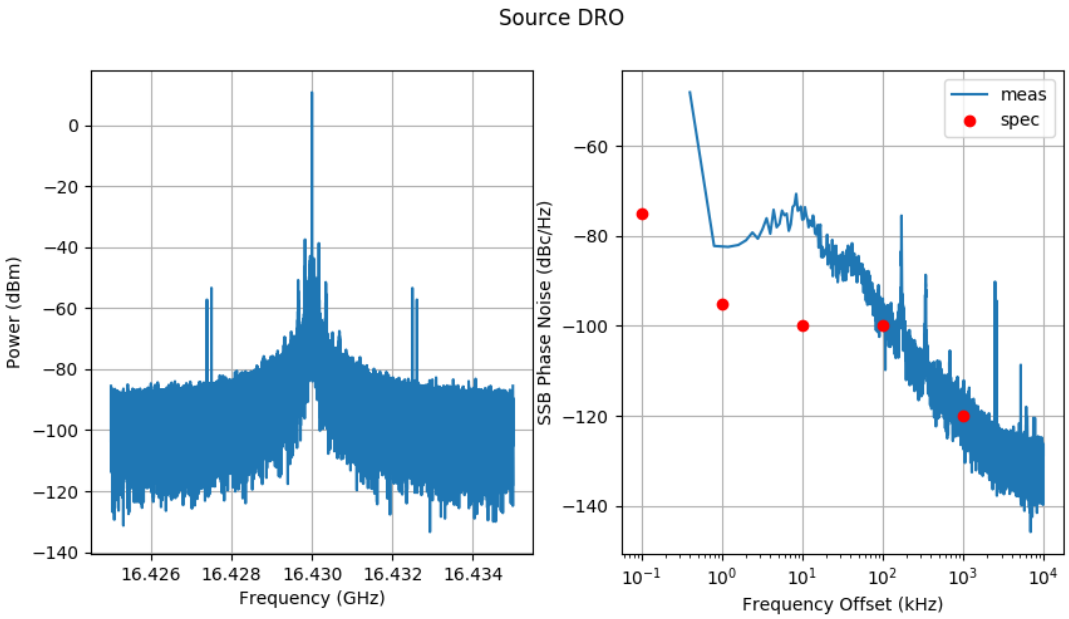

(b)

Figure 4.8: (a) Power spectrum of 12 GHz DRO (left), and its conversion to phase noise (right). (b) Power spectrum of 16 GHz DRO (left), and its conversion to phase noise (right).

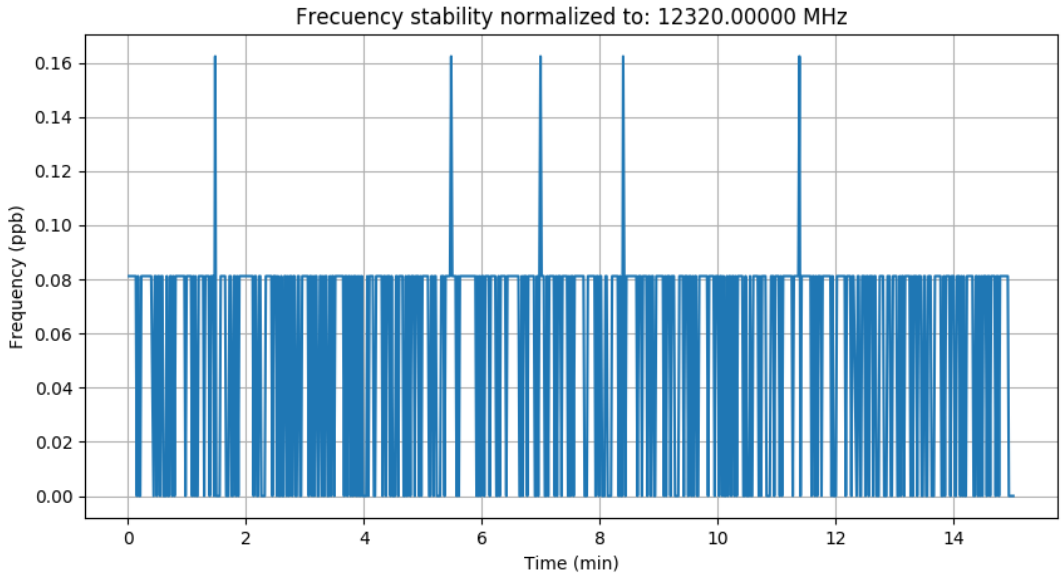

(a)

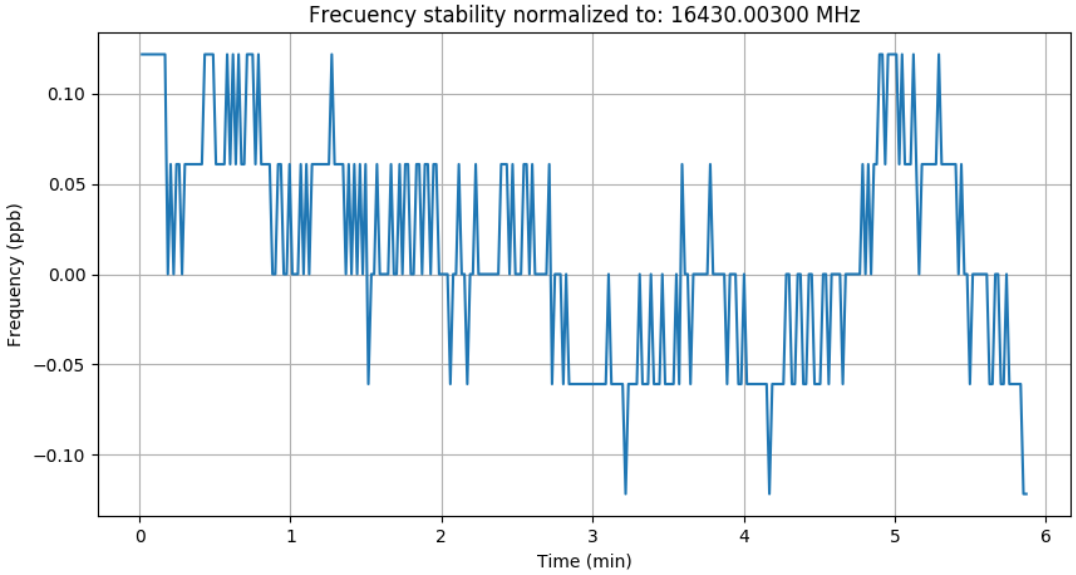

(b)

Figure 4.9: (a) Normalized frequency stability of the 12 GHz DRO. (b) Normalized frequency stability of 16 GHz DRO.

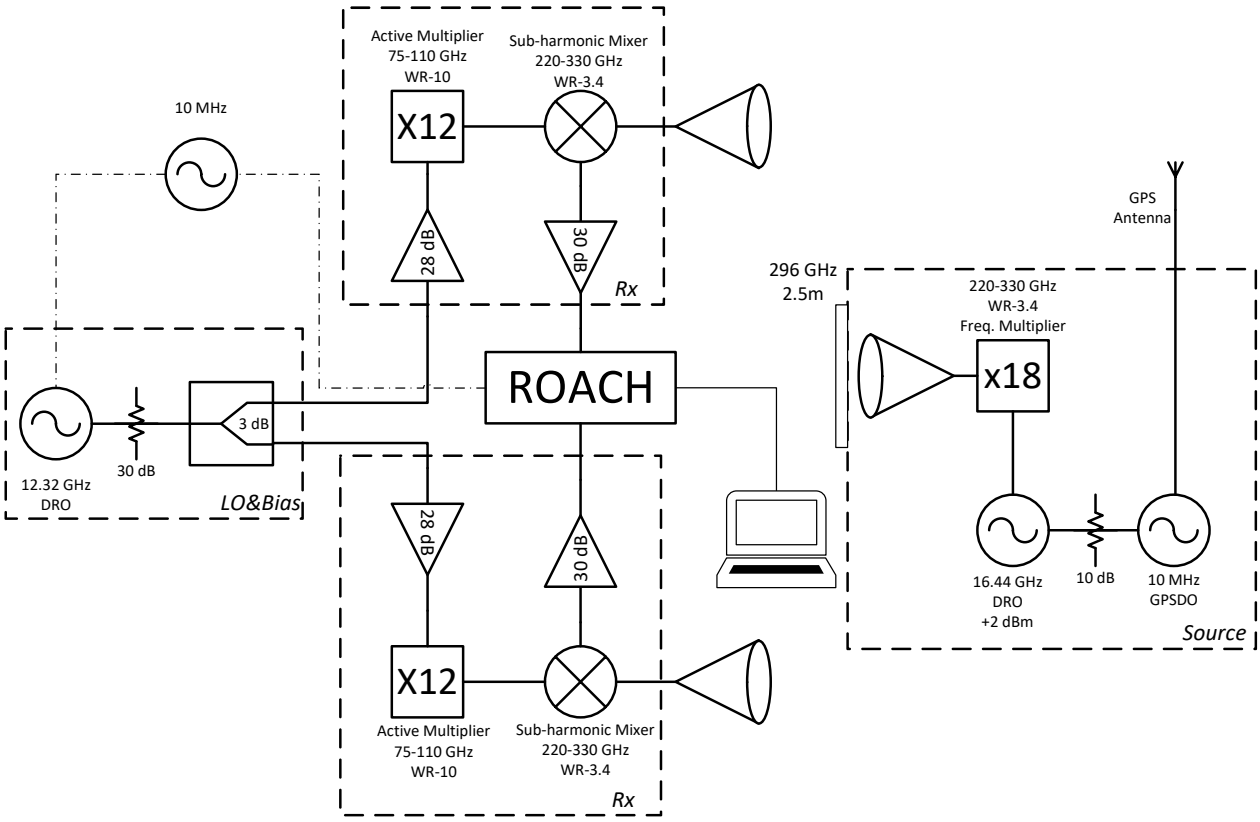

Figure 4.10: Setup schematics for the end-to-end test. The source (right) is emitting a 296 GHz signal, which is phase locked using the GPS signal. Two receivers capture the signal using the final horns and electronics. The 60 MHz IF signals are fed into the ROACH back-end, which computes their magnitudes and phase difference. The local oscillator and ADC clocks are both locked to a laboratory instrument 10 MHz standard.

4.4. End-to-end tests

As the names implies, the purpose of this test is to evaluate the behaviour of the whole system, with emphasis in quantifying its stability. The setup, described in Figure 4.10, was assembled at the laboratory and a rough alignment of the source was performed, leaving both receivers with the same power level. For simplicity both receivers were static and bolted to an optical table, therefore, any mapping is left out of the scope of the test. The back-end was configured to have a sampling rate of 1.2 ms and the data is momentarily stored in a ring buffer inside the FPGA, from where it is dumped to a file every 20 minutes. This file is managed by the ROACH operative system, which runs on a Power-PC microcontroller. Finally, this data is then transferred via Ethernet to a monitoring computer, which runs a python code. The timestamp subsystem of the correlator could not be used, since the only equipment with an IRIG-code output did not have a stable 10 MHz reference. Also, a 30 dB attenuator was used to lower the power of the local oscillator, to emulate the losses of the final cables and enable the use of the LO amplifiers in each receiver. This setup was left running during the night, since the system was found to be sensitive to drafts of air.

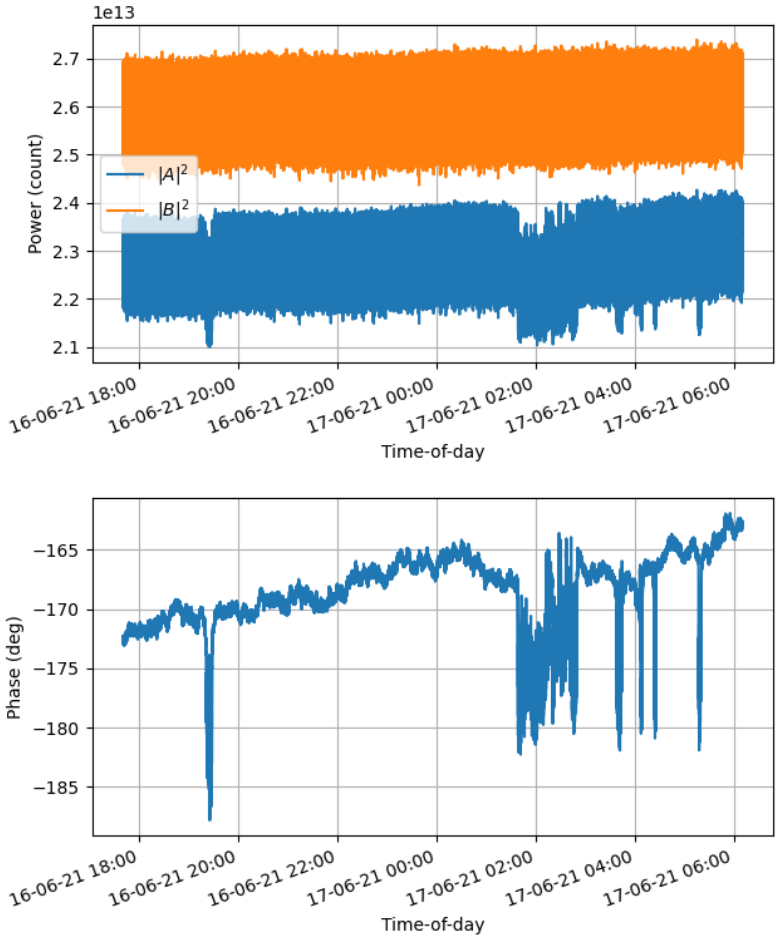

Figure 4.11: Plot of the overnight system behaviour. In the upper graph is the direct reading of the A and B channels of the correlator, in linear scale. And, in the lower graph, the calculated phase difference using readings from the complex cross-correlation reading.

The results of the test are shown in Figure 4.11 for one continuous measurement. From the graphs it is clear that the system exhibits "jumps" in both phase and amplitude, i.e., sudden changes that are not attributable to thermal drift. Though the final system considers to calibrate multiple times during one measurement, this jumps are not acceptable to ensure the reliability of the system. Simple checks were performed like the strength of the connections, the effect of movement of the cables and the value of the bias voltages. None of these replicated the observed jumps.

A probable cause for this behaviour is a stability issue with one of the DRO units, more specifically the internal PLL unit being unable to maintain lock with the 10 MHz signal. This could not be verified, though, due to time constraints because the only interface that reported lock status was a TTL signal, which required additional hardware to be logged. It needs to be noted that the "jumps" are relatively small, and this final test was the first setup implemented with enough sensitivity at 300 GHz to detect them.

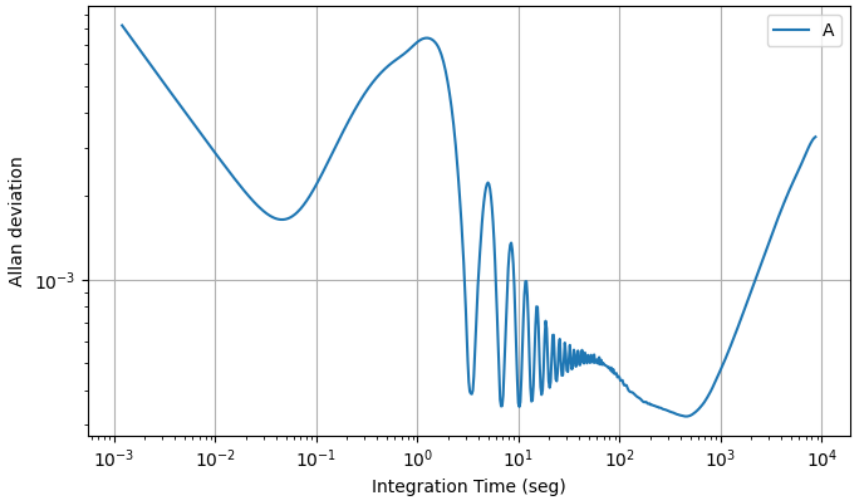

Figure 4.12: Allan deviation of the power channel of one of the signals, using data from the overnight measurement. The return point is in the order of the 300 seconds.

To continue the analysis of this test only data from without jumps will be considered, or more precisely, the data of the longest working time without jumps will be used. This assumes that the system is representative of the final behavior on that period, but such argument could not be proved, due to time constraints of the project. Further analysis would need to be carried out in Germany.

The stability of the system was studied by taking the Allan variance of one of the channels, over the aforementioned window of data. The result is shown in Figure 4.12, using the Overlapping Allan Variance method, which gives an improved confidence of the estimation. From this curve it can be seen that the return point is around 300 seconds, or 5 minutes. This can be considered acceptable for the final operation, although the scan time is expected to be 20 minutes, the multiple calibrations can account for the drift of less than 5 minutes. Also, a strong oscillation can be observed in the curve, which points to an amplitude modulation of the signal [25]. This can be corroborated with the computation of the Fourier transform of the signal, which is shown in Figure 4.13, where the fundamental frequency is around 0.3 Hz or a period of 3.3 seconds. Furthermore, it can be deduced that the oscillation comes from the source because the ratio of both channels does not exhibit such harmonics.

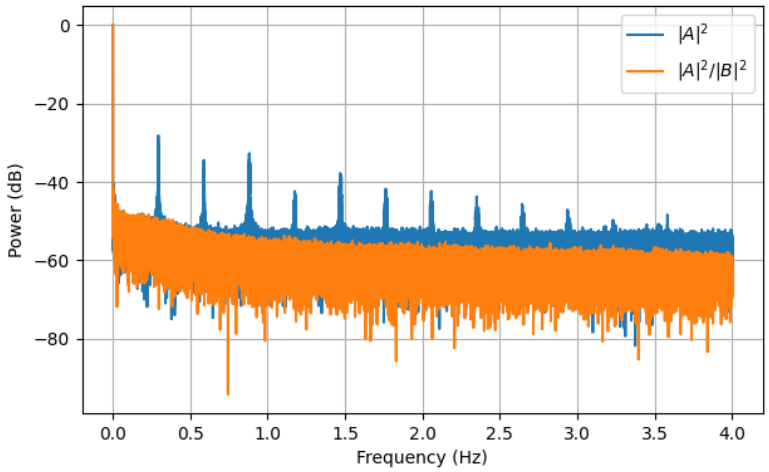

Figure 4.13: Power spectrum of the power channel, computed with data from the overnight measurement. In blue is the spectrum of the power of one channel, in red is the spectrum of the ratio of the power of both channels.

4.5. Summary

The various tests performed to characterize the system are presented in this chapter. The anechoic chamber of the Millimeter Wave Laboratory was upgraded to perform measurements at 300 GHz. This was used to confirm that the conical-spline horn was compliant with electromagnetic simulations. The transmission of the Goretex membrane was measured, obtaining 0.07 dB at 295.6 GHz. The Dielectric Resonant Oscilators were also characterized by measuring a frequency stability better that ±0.2 ppb and finding that, in terms of phase noise, the 12 GHz oscillator for the dual receiver complies with specifications, but not the 16 GHz oscillator for the source. The integration of the system was tested to evaluate its overall stability, estimating an Allan time of 5 minutes approximately. Finally, some issues were discovered in the integration test that need to be addressed. First, an amplitude modulation of 0.3 Hz was found in the source 300 GHz signal. Second, a sporadic switching type of instability was found that could not be identified, due to time constraints.

Chapter 5

Conclusions and Future Work

This thesis accomplished its objectives about the design, implementation, characterization and testing of the hardware necessary for the development of a 300 GHz holography system for FYST. The design covers the complete source the auxiliary electronics and part of the receivers.

The anechoic chamber at the Millimeter Wave Laboratory was successfully upgraded for 300 GHz measurements. This allowed to validate the design of the horn antenna, which impacts drastically in the optical system. Also this data is fundamental for the holography system, as it is used in the novel fitting algorithm that computes the reflector surface deviations.

A phase stable 300 GHz source was designed and assembled, its stainless steel enclosure ensures that no corrosion will develop in the event of being covered by snow. Also, it was proven in the laboratory that it can use the GPS signal to maintain phase coherency, as discussed in section 4.4. After integrating the whole system it was determined that it has a stability that satisfies the requirements of Table 2.4. This was quantified by computing an Allan time of 300 seconds, or 5 minutes. However, some problems were detected in the system that will require further testing and developing. This were the oscillations present in the signal emitted by the source and the sporadic instabilities encountered on the end-to-end test.

The remaining design, in particular the enclosure and optics of the receivers, will be completed by the team at University of Cologne. Also, by the same team, an experiment will be developed to obtain the surface deviations of a scaled version of the telescope's reflectors.

Future work should continue the characterization of the system, such as the measurement of the absolute power generated by the source, the measurement of the cross-polarization radiation pattern of the horn antenna and the measurement of the source beam pattern. Also, it is important to verify that the source is capable to withstand outdoor weather conditions. All this should be done before the tests using FYST's optical system, to be able to account for systematic errors.

This work is one step more needed to obtain the first holography system at 300 GHz

for radio telescopes, with an accuracy five times better than all previous implementations. Another notable characteristic of this thesis is the collaboration between University of Chile and the Fred Young Telescope. Finally, it is important to mention that this work has already produced a conference paper in the Society of Photo-Optical Instrumentation Engineers (SPIE) [26], an it is expected to produce another publication when the capabilities of the system are proven experimentally.

BIBLIOGRAPHY

[1] J. Ruze, "Aperture tolerance theory - a review," in *1965 Antennas and Propagation Society International Symposium*, vol. 3, pp. 210–210, 1965.

[2] K. Rohlfs and T. L. Wilson, *Tools of radio astronomy*. Springer Science & Business Media, 2013.

[3] M. Kesteven, B. Parsons, and D. Yabsley, "Antenna reflector metrology: the australia telescope experience," *IEEE transactions on antennas and propagation*, vol. 36, no. 10, pp. 1481–1484, 1988.

[4] J. Baars, R. Lucas, and J. Mangum, "Near field radio holography of the ALMA prototype antennas." [Online] https://www.mrao.cam.ac.uk/~richard/Antenna_Measurement/ALMAmemo.pdf, 2004. [Accessed: Sept-05-19].

[5] M. Kesteven, "Photogrammetry for large structures." [Online] https://www.gb.nrao.edu/MetConf/talks/Wednesday/Kesteven.pdf, 2016. [Accessed: Oct-25-21].

[6] C. A. Balanis, *Antenna theory: analysis and design*. John wiley & sons, 2015.

[7] D. Morris, "Phase retrieval in the radio holography of reflector antennas and radio telescopes," *IEEE transactions on antennas and propagation*, vol. 33, no. 7, pp. 749–755, 1985.

[8] W. Reich and E. Fürst, *Holographic measurements of the Effelsberg 100-m Radiotelescope via Phase Retrieval*. Max-Planck-Inst. für Radioastronomie, 1999.

[9] D. Morris, M. Bremer, G. Butin, M. Carter, A. Greve, J. Lamb, B. Lazareff, J. Lopez-Perez, F. Mattiocco, J. Penalver, *et al.*, "Surface adjustment of the IRAM 30 m radio telescope," *IET microwaves, antennas & propagation*, vol. 3, no. 1, pp. 99–108, 2009.

[10] D. J. Rochblatt, "Holographic measurements of the NASA-JPL Deep Space Network antennas," in *1998 IEEE Aerospace Conference Proceedings (Cat. No. 98TH8339)*, vol. 3, pp. 441–452, IEEE, 1998.

[11] B. Nikolic, R. Prestage, D. Balser, C. Chandler, and R. Hills, "Out-of-focus holography at the Green Bank Telescope," *Astronomy & Astrophysics*, vol. 465, no. 2, pp. 685–693, 2007.

[12] J. Baars, R. Lucas, J. Mangum, and J. Lopez-Perez, "Near-field radio holography of large reflector antennas," *IEEE Antennas and Propagation Magazine*, vol. 49, no. 5, pp. 24–41, 2007.

[13] L. R. D'Addario, "Holographic antenna measurements: further technical considerations," *12m Telescope Memo No. 202, NRAO*, 1982.

[14] H. Kiuchi, M. Yamada, M. Sugimoto, H. Saito, T. Matsui, and M. Saito, "A holography receiver design for the ALMA submillimeter antenna surface measurement," *IEEE Transactions on Instrumentation and Measurement*, vol. 62, no. 10, pp. 2763–2772, 2013.

[15] S. C. Parshley, J. Kronshage, J. Blair, T. Herter, M. Nolta, G. J. Stacey, A. Bazarko, F. Bertoldi, R. Bustos, D. B. Campbell, *et al.*, "CCAT-prime: a novel telescope for sub-millimeter astronomy," in *Ground-based and Airborne Telescopes VII*, vol. 10700, p. 107005X, International Society for Optics and Photonics, 2018.

[16] R. Bustos, M. Rubio, A. Otárola, and N. Nagar, "Parque astronómico de atacama: An ideal site for millimeter, submillimeter, and mid-infrared astronomy," *Publications of the Astronomical Society of the Pacific*, vol. 126, no. 946, p. 1126, 2014.

[17] S. C. Parshley, M. Niemack, R. Hills, S. R. Dicker, R. Dünner, J. Erler, P. A. Gallardo, J. E. Gudmundsson, T. Herter, B. J. Koopman, *et al.*, "The optical design of the six-meter CCAT-prime and Simons Observatory telescopes," in *Ground-based and Airborne Telescopes VII*, vol. 10700, p. 1070041, International Society for Optics and Photonics, 2018.

[18] C. Medina Porcile, "CCAT-prime telescope holography simulations and surface error analysis," Master's thesis, Universidad de Chile, 2019.

[19] S. A. Jorquera Tapia, *Diseño, implementación y pruebas de voltímetro vectorial en plataforma basada en FPGA para mediciones de holografía del Telescopio CCAT-prime.* Engineering thesis, Universidad de Chile, 2020.

[20] D. A. Montofré, R. Molina, A. Khudchenko, R. Hesper, A. M. Baryshev, N. Reyes, and F. P. Mena, "High-performance smooth-walled horn antennas for THz frequency range: Design and evaluation," *IEEE Transactions on Terahertz Science and Technology*, vol. 9, no. 6, pp. 587–597, 2019.

[21] International Telecommunication Union, "Passive bands of scientific interest to EESS/SRS from 275 to 3000 GHz." [Online] https://www.itu.int/pub/R-REP-RS.2194-2010, 2010.

[22] H. J. Gibson, B. Thomas, L. Rolo, M. C. Wiedner, A. E. Maestrini, and P. de Maagt, "A novel spline-profile diagonal horn suitable for integration into thz split-block components," *IEEE Transactions on Terahertz Science and Technology*, vol. 7, no. 6, pp. 657–663, 2017.

[23] P. F. Goldsmith *et al.*, *Quasioptical systems.* Chapman & Hall New York, 1998.

[24] P. N. Betjes, "An algorithm for automated phase center determination and its implementation," in *Proc. Antenna Meas. Technol. Assoc. Annu. Symp.*, pp. 1–6, 2007.

[25] W. J. Riley, *Handbook of frequency stability analysis.* US Department of Commerce, National Institute of Standards and Technology, 2008.

[26] X. Ren, P. Astudillo, U. U. Graf, R. E. Hills, S. Jorquera, B. Nikolic, S. C. Parshley, N. Reyes, and L. Weikert, "Holographic surface measurement system for the fred young submillimeter telescope," in *Ground-based and Airborne Telescopes VIII*, vol. 11445, pp. 1129–1147, SPIE, 2020.